

CERN-EP-2018-320
2019/12/18

CMS-SMP-17-001

Measurement of the differential Drell–Yan cross section in proton-proton collisions at $\sqrt{s} = 13$ TeV

The CMS Collaboration*

Abstract

Measurements of the differential cross section for the Drell–Yan process, based on proton-proton collision data at a centre-of-mass energy of 13 TeV, collected by the CMS experiment, are presented. The data correspond to an integrated luminosity of 2.8 (2.3) fb^{-1} in the dimuon (dielectron) channel. The total and fiducial cross section measurements are presented as a function of dilepton invariant mass in the range 15 to 3000 GeV, and compared with the perturbative predictions of the standard model. The measured differential cross sections are in good agreement with the theoretical calculations.

"Published in the Journal of High Energy Physics as doi:10.1007/JHEP12(2019)059."

arXiv:1812.10529v2 [hep-ex] 17 Dec 2019

1 Introduction

Drell–Yan (DY) production of same-flavour, oppositely charged lepton pairs in proton-proton collisions occurs via the s -channel exchange of γ^*/Z bosons. Current theoretical predictions for the cross section are accurate up to next-to-leading order (NLO) in the electroweak (EW) coupling and up to next-to-next-to-leading order (NNLO) in perturbative quantum chromodynamics (QCD) [1–4]. Hence, a precision measurement of the differential cross section for the DY process at the LHC provides an important test of the perturbative framework of the standard model (SM). In a complementary way, the experimental results can also be used to constrain the parton distribution functions (PDFs). DY production of dileptons is also a major source of background for rare SM processes as well as searches for physics beyond the SM. Hence, it is important to measure the DY production rate accurately up to the largest accessible energy.

The single- and double-differential cross sections, $d\sigma/dm$ and $d^2\sigma/dmd|y|$, where m is the dilepton invariant mass and $|y|$ is the absolute value of the dilepton rapidity, were previously measured by the ATLAS [5–7] and CMS [8–10] Collaborations in proton-proton (pp) collisions for the centre-of-mass energy $\sqrt{s} = 7$ and 8 TeV at the LHC. Using early data collected in 2015 at $\sqrt{s} = 13$ TeV and corresponding to an integrated luminosity (\mathcal{L}) of 81 pb^{-1} , the ATLAS Collaboration measured the Z production cross section times branching ratio of $Z \rightarrow \ell^+\ell^-$ near the resonance region [11]. This paper presents the first measurement of the DY spectrum $d\sigma/dm$ over a wider invariant mass range using 2015 pp collision data collected by the CMS Collaboration at $\sqrt{s} = 13$ TeV at the LHC, corresponding to $\mathcal{L} = 2.8$ (2.3) fb^{-1} in the dimuon (dielectron) channel. The range of x , the momentum fraction carried by an interacting parton, covered by this measurement is $10^{-4} < x < 1.0$.

The cross section as a function of invariant mass for a specific bin i is determined by the following relation:

$$\sigma_i = \frac{N_i}{A_i \varepsilon_i \rho_i \mathcal{L}}, \quad (1)$$

where N_i denotes the signal yield in a given bin i after subtracting the background. It is obtained using an unfolding technique to correct for the detector resolution effects and final-state photon radiation (FSR). The acceptance A_i and the experimental efficiency ε_i are obtained from the Monte Carlo (MC) simulation. A scale factor ρ_i accounts for any difference in the efficiency between data and simulation.

2 The CMS detector

The central feature of the CMS apparatus is a superconducting solenoid of 6 m internal diameter, providing a magnetic field of 3.8 T. Within the solenoid volume are a silicon pixel and strip tracker, a fine-grained and hermetic crystal electromagnetic calorimeter (ECAL), and a sampling hadron calorimeter, each composed of a barrel and two endcap sections. Extensive forward calorimetry with lead and quartz-fibre Cherenkov detectors complement the coverage provided by the barrel and endcap detectors. Muons are measured in gas-ionisation detectors using three technologies: drift tubes, cathode strip chambers, and resistive-plate chambers embedded in the steel flux-return yoke outside the solenoid.

The ECAL consists of about 76k lead tungstate crystals, which provide a coverage in pseudorapidity $|\eta| < 1.479$ in the barrel region and $1.566 < |\eta| < 2.5$ in two endcap regions (EE). A preshower detector consisting of two planes of silicon sensors interleaved with a total of $3X_0$ of lead is located in front of EE. The momentum of an electron candidate is estimated by combining the measurements in the ECAL and tracker. The resolution of transverse momentum (p_T)

for electron candidate with p_T about 45 GeV, ranges from 1.7% for nonshowering electrons in the barrel region to 4.5% for showering electrons in the endcaps [12].

Muons are measured in the range $|\eta| < 2.4$. Matching the track of a muon candidate to that measured in the silicon tracker results in a p_T resolution of 1.3–2.0% in the barrel and better than 6% in the endcaps for muons with $20 < p_T < 100$ GeV. The resolution is better than 10% for muons with p_T up to about 1 TeV [13].

The first level of the CMS trigger system [14], composed of custom hardware processors, uses information from the calorimeters and the muon detector to select the most interesting events at a level of 1 in 10^4 within $4 \mu\text{s}$. The high-level trigger, consisting of processor farms, uses the complete information from the detector to reconstruct the event and discriminate further to reduce the selection rate to less than about 1 kHz, before data storage. A more general description of the CMS detector with a definition of the coordinate system used and the relevant kinematic variables, can be found in Ref. [15].

3 Data sets and simulated event samples

The collision data used in this analysis is collected with an inclusive single-muon (electron) trigger. The events in the dimuon channel are triggered by the presence of at least one muon candidate with $p_T > 20$ GeV and $|\eta| < 2.4$. The events for the dielectron channel are triggered by an electron with $p_T > 23$ GeV and $|\eta| < 2.5$, satisfying loose identification and isolation criteria.

Various MC samples are used to simulate the DY signal and background processes. The MADGRAPH5_aMC@NLO v2.2.2 [16] event generator is used to simulate the signal and W production in association with one or more jets (W+jets) events at NLO accuracy in the QCD coupling constant, α_s . Pair production of top quarks ($t\bar{t}$) and single top quark production in association with a W boson (tW and $\bar{t}W$) are generated at NLO using POWHEG v2.0 and v1.0 respectively [17–21]. Diboson processes (WW, WZ, and ZZ) are simulated at leading order with PYTHIA v8.212 [22]. All samples are generated with the PDF package of NNPDF3.0 [23, 24]. The PYTHIA generator with the underlying event tune CUETP8M1 [25] is used for the showering and hadronisation in all samples. For simulations at NLO, jets from matrix element calculations and parton showering are merged using the FxFx prescription [26]. The total production rate for each process is normalised using the most accurate theoretical cross section value available. The DY process is normalised to the predicted cross section calculated using the MADGRAPH5_aMC@NLO. The $t\bar{t}$ rate is normalised to the predicted cross section using a calculation performed with NNLO+NNLL (next-to-next-to-leading logarithm) accuracy [27]. The normalisations for the single top quark and diboson samples use cross section values available at NLO accuracy [28, 29].

In all the MC samples, the detector response is simulated using a detailed description of the CMS detector based on the GEANT4 [30] package. The simulated events are reconstructed using the same software as the real data. Minimum bias events are superimposed on the simulated physics processes to emulate the effects of multiple interactions per bunch crossing (pileup); typically an average number of 11. All MC samples are reweighted to provide the same pileup distribution observed in the data.

4 Event selection

Each reconstructed offline muon candidate is required to meet identification criteria that are based on the number of hits found in the tracker, the response of the muon detectors, and a set of criteria based on the matching between the muon track parameters as measured by the inner tracker and muon detectors. Furthermore, the two muon candidates are required to share a well-defined common vertex. To reject cosmic ray muons that can appear to be back-to-back muon pairs, the transverse impact parameter with respect to the centre of the interaction region is required to be small and the opening angle between the two candidates should be differ from π by more than 5 mrad. In order to suppress nonprompt muon candidates from heavy flavour decays, muons are required to be well-isolated within a cone of size $\Delta R = 0.3$, where $\Delta R = \sqrt{(\Delta\eta)^2 + (\Delta\phi)^2}$. More details on the muon reconstruction, identification and isolation criteria used in this analysis can be found in Refs. [13].

The offline reconstructed electron candidates are required to pass identification criteria that are based on electromagnetic shower shape variables. Electron candidates originating from photon conversions are suppressed by requiring that they have at most two missing inner tracker hits and that they are not consistent with being part of a conversion pair. The isolation of an electron candidate is defined by measuring the sum of energy deposits associated with the photons as well as with the charged and neutral hadrons reconstructed by the particle-flow (PF) algorithm [31] with the same cone size as for the muons. The electron selection is based on the ratio of the PF isolation to the p_T of the electron candidate. More details about electron reconstruction and identification criteria used in this analysis are given in Refs. [12, 32].

For the offline analysis the leading muon (electron) candidate in the event is required to have $p_T > 22$ (30) GeV and the subleading candidate $p_T > 10$ GeV. All muon candidates are required to satisfy $|\eta| < 2.4$, and all electron candidates should satisfy $|\eta| < 2.5$, while excluding the barrel-endcap transition region of the ECAL ($1.44 < |\eta| < 1.57$). The two muon candidates are required to have opposite charges, and the pair with the best fit of the dimuon vertex is selected if there is more than one candidate pair in the same event. No opposite-charge and same-vertex requirements are applied in the dielectron channel to avoid a selection inefficiency. At least one of the two candidate leptons, selected in the event, is required to match the object that triggered the events.

The reconstructed dilepton invariant mass distribution can be affected by an imperfect measurement of the momentum and energy of the lepton candidates. Momentum scale corrections for the muons are applied using the procedures described in Refs. [10, 33]. The electron energy deposits, as measured in ECAL, are subject to a set of corrections involving information from both the ECAL and tracker [12, 32].

The measurements are performed in 43 bins of dilepton invariant mass. The binning at $m < 600$ GeV is identical to that used in the earlier measurement [10], although the highest bin is extended to 3000 GeV. The highest mass events observed in the data set are about 2.3 TeV in both channels.

5 Background estimation

The background composition varies across the dilepton invariant mass range, with the dominant backgrounds over the entire mass range being $t\bar{t}$, tW , and $\bar{t}W$ production, except for the region below the Z boson peak, where DY production of $\tau^+\tau^-$ pairs and their subsequent decays to electron and muon pairs constitute a significant background. In the dimuon channel,

the QCD multijet background is relatively large at low mass, below about 60 GeV. However, in the dielectron channel, it contributes significantly in the high mass region as well.

The main backgrounds are estimated from data using control samples to reduce the systematic uncertainty due to the imperfect knowledge of the theoretical cross sections for the SM processes. For $t\bar{t}$, tW , $\bar{t}W$, $\tau^+\tau^-$, and WW production, the contributions are estimated from a large data sample containing electron-muon pairs of opposite charge; the identification criteria used to select this sample are the same used to select the signal samples (described in the previous section). The rates are twice as large as those for dimuon or dielectron events; however, the contributions of the same-flavour final states are scaled after correcting for the relevant detector acceptance and efficiency.

The QCD multijet and W +jets processes contribute to the background mainly when one or more jets are misidentified as electron or (less likely) as muon candidates; the contributions are estimated using the “misidentification rate” method described in Refs. [9, 34]. The misidentification rate is measured as a function of muon and electron p_T in the barrel and endcap regions separately. Subsequently, the misidentification rate is applied to events with loosely isolated leptons, after subtracting the contributions of genuine dilepton events. The contributions from genuine lepton candidates from DY and $t\bar{t}$ production are subtracted using a lepton distribution fit obtained from the simulation. The misidentification rate in the dimuon channel is defined as the ratio of the number of isolated muon candidates passing the muon identification criteria and the number of muon candidates passing the muon identification with no isolation requirement. For this measurement a data sample selected with the single-muon trigger is used. The definition of the misidentification rate in the dielectron channel is slightly different and is calculated by measuring the probability of a jet passing the final electron selection criteria described above. For this measurement, a large unbiased event sample has been used, selected with a combination of single-photon triggers rather than electron triggers. The fraction of misidentified lepton backgrounds is generally less than 1% across the entire mass range in the dimuon channel and up to 3% (5%) below (above) the Z boson peak in the dielectron channel.

The contribution from WZ and ZZ processes are evaluated using simulation. The photon-initiated (PI) production of same-flavour lepton pairs is estimated with the FEWZ 3.1 package [35, 36], using the LUXqed photon PDF [37]. Events generated with PYTHIA are used in the MRST2004qed PDF set as a cross-check [38]. The contributions from PI production are negligible, except in the high mass region [39].

Figure 1 presents the dilepton invariant mass distributions in dimuon and dielectron channels. The cumulative yields from the signal and the background discussed above are superimposed on the data.

6 Corrections

To compare the measured distributions with the theoretical predictions, various experimental corrections need to be applied after subtracting the total expected background from the observed number of events in each mass bin. The correction for the detector resolution effects is implemented using an unfolding technique, similar to that used in the previous measurement [10]. The event acceptance and selection efficiency are estimated using simulation and are used to correct the data. Any difference in the selection efficiency between the data and simulation is corrected for using a scale factor. Finally, the correction required to account for the effects of FSR on the invariant mass of the lepton pair is applied, using so-called “dressed

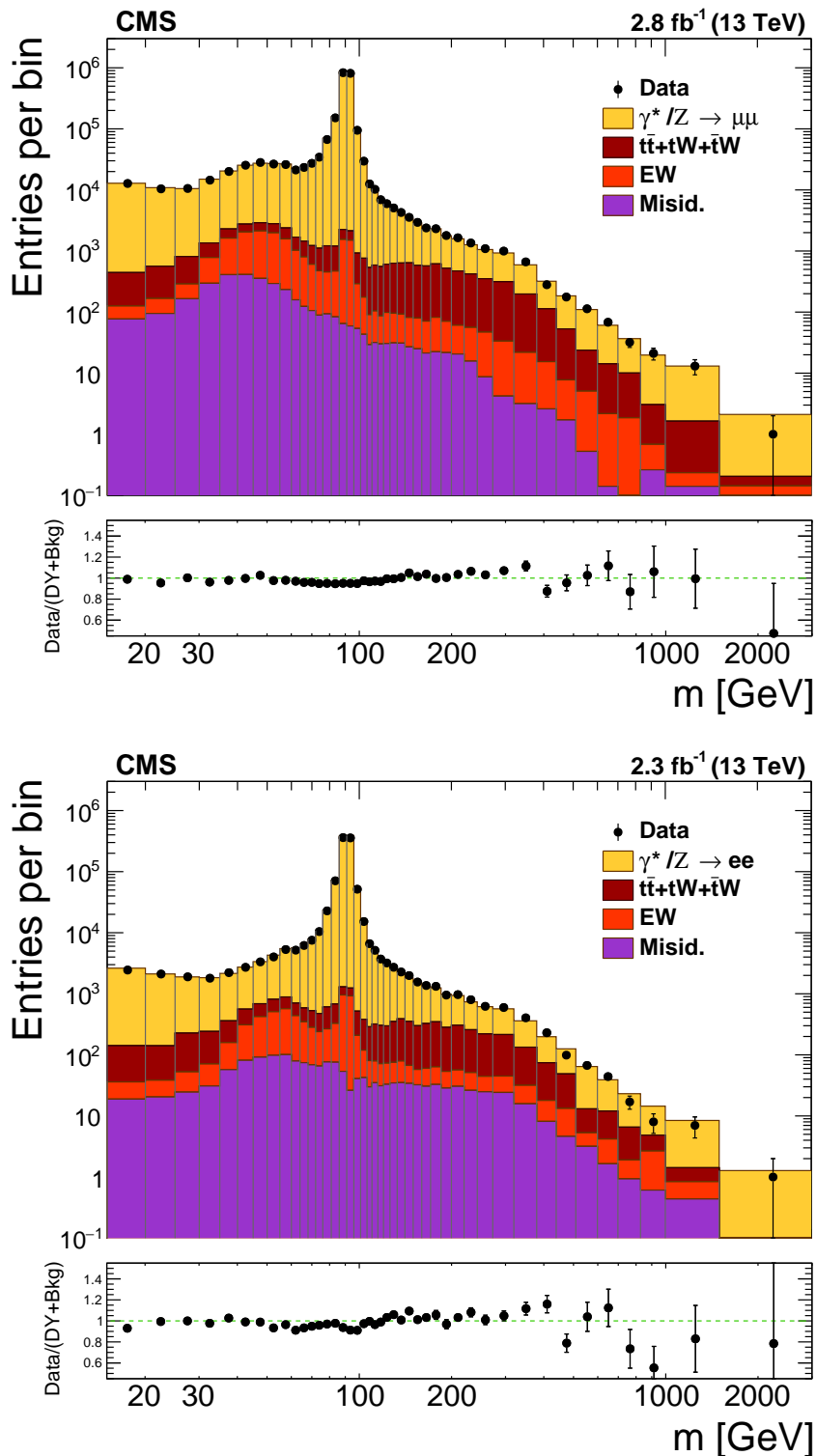


Figure 1: The observed dimuon (top) and dielectron (bottom) invariant mass spectra within the detector acceptance. The “EW” label indicates the contributions from the DY production of $\tau^+\tau^-$, WW, WZ, and ZZ processes. The “Misid.” label corresponds to W +jets and QCD multijet backgrounds. Each MC process is normalised using the most accurate theoretical cross section value available. The error bars on the data points represent the statistical uncertainty only.

leptons” and further unfolding. The details of the correction procedures are discussed below.

6.1 Detector resolution effects

The detector resolution occasionally leads to migration of events from mass bin k of the generator level distribution to another bin i of the reconstructed distribution. This effect is corrected by unfolding using the iterative D’Agostini method [40] with a response matrix. The iteration is terminated when the difference between the result and the previous one is less than 0.1% in the entire mass bin. The validity of the unfolding method is tested on simulated events.

The elements of the detector response matrix, T_{ik} , are calculated using the DY simulation sample. Each element contains the fraction of events that migrated from the k th bin of the generator level (the post-FSR level, described in Section 6.4) mass distribution to the i th bin of the reconstructed mass distribution, such that

$$N_{\text{obs},i} = \sum_k T_{ik} N_{\text{gen level},k}. \quad (2)$$

The effect of the unfolding on the differential cross section is largest in the Z boson peak region because of the narrow width, where the effect on the signal yield is observed as large as 30 and 40% in the dimuon and dielectron channels, respectively.

6.2 Acceptance and efficiency

The acceptance is defined as the fraction of simulated signal events with both leptons passing the nominal p_T and η requirements of the analysis mentioned in Section 4, with respect to the full phase space. The efficiency is defined as the fraction of simulated signal events that lie within the acceptance and that satisfy all the event selection criteria. The following equation defines the acceptance and efficiency for a given mass bin:

$$A \varepsilon = \frac{N_A}{N_{\text{gen}}} \frac{N_\varepsilon}{N_A}, \quad (3)$$

where N_{gen} is the total number of generated signal events, N_A is the number of events passing the acceptance criteria, and N_ε is the number of reconstructed events passing the full event selection. Figure 2 shows the variation of the acceptance and efficiency as functions of the dilepton invariant mass in the dimuon and dielectron channels. The acceptance correction is not applied to the fiducial cross section, but it is applied to the result in the full phase space, as described in Section 8.

6.3 Efficiency correction

To correct for the difference in efficiencies between data and simulation for lepton reconstruction, identification, isolation, and trigger, scale factors are determined from the data using the “tag-and-probe” method [41]. Events are selected that contain a dilepton pair near the resonance region where the background is very small. One lepton is required to satisfy the tight selection and the other is used as the probe lepton. The efficiency is then determined from the number of probe leptons that also pass the required selection criteria. The measured efficiency using the tag-and-probe method is parametrised as a function of lepton p_T and η and is then factorised into the reconstruction, identification, and isolation related components. The overall efficiency is then given by

$$\varepsilon_{\text{event}} = \varepsilon_{\ell_1} \varepsilon_{\ell_2} \varepsilon_{\text{event, trig}}, \quad (4)$$

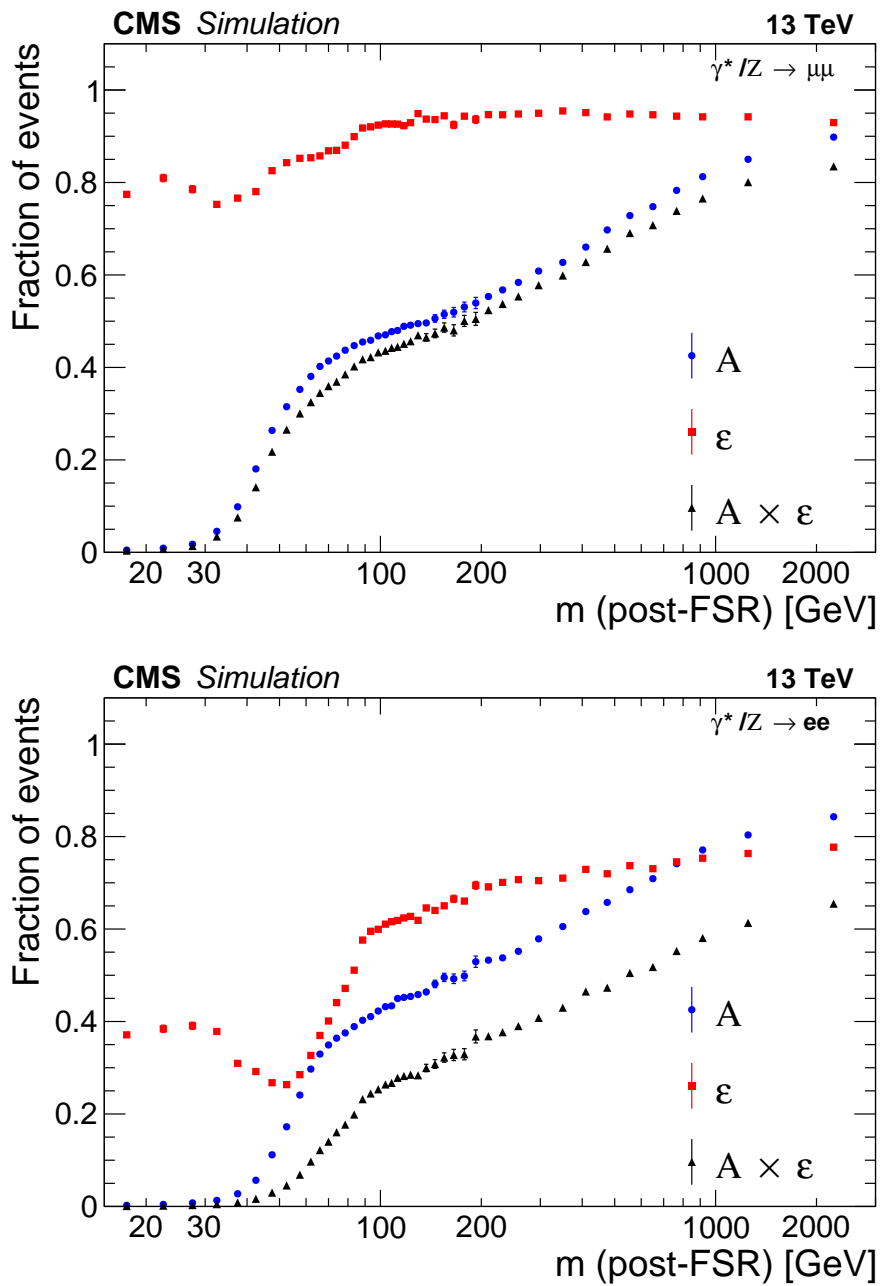


Figure 2: The signal acceptance (A), efficiency (ϵ) and their product for each invariant mass bin in the dimuon (top) and dielectron (bottom) channels, calculated from simulation. The error bars on the data points represent the statistical uncertainty only.

where $\varepsilon_{\ell_{1,2}}$ are the single-lepton efficiencies of the individual leptons and $\varepsilon_{\text{event, trig}}$ is the trigger efficiency for the event [9, 10].

The scale factor between data and simulation is determined by the ratio $\varepsilon_{\text{data}}(\text{event})/\varepsilon_{\text{MC}}(\text{event})$. The scale factors are measured to be 0.92–0.97 (0.95–0.97) in the dimuon (dielectron) channel; the values are dependent on the data-taking period. The scale factors are then applied to the simulation to correct for the observed differences.

6.4 Final-state photon radiation effects

The FSR from a lepton shifts the measured invariant mass of the dilepton pair to lower values, which significantly affects the distribution below the Z boson peak, especially in the dielectron channel. The definition of “dressed lepton” accounts for the required correction for a given flavour so that the results from the individual channels can be combined subsequently for comparison with the theoretical predictions. The four-momentum of the “dressed lepton” is defined as

$$p_{\ell}^{\text{dressed}} = p_{\ell}^{\text{post-FSR}} + \Sigma p_{\gamma}, \quad (5)$$

where the four-momenta of all the simulated photons originating from the leptons are summed within a cone of $\Delta R < 0.1$ around the candidate lepton, where ΔR is the separation of the photon from the lepton in η - ϕ space. This enables to correct the lepton momentum to compensate missing momentum due to the FSR.

The FSR correction is estimated separately using an unfolding technique from a signal MC sample where the FSR is simulated by PYTHIA. The response matrix is produced using the information about dressed and post-FSR leptons in the simulation. The correction to the cross section, defined in terms of dressed leptons using data corresponding to a post-FSR lepton, is in the range of 0.78–1.09 (0.58–1.27) in the dimuon (dielectron) channel. The FSR correction is not applied to the fiducial cross section, but it is applied to the result in the full phase space described in Section 8.

7 Systematic uncertainties

Systematic uncertainties are the dominant source of the total uncertainty in this measurement for $m < 400$ GeV.

In the dimuon channel, the efficiency scale factor (which includes muon reconstruction, identification, isolation, and trigger selection) is the most significant component of the systematic uncertainty below the Z boson peak. A variety of possible contributions to the efficiency scale factor are listed:

- statistical uncertainty associated with the tag-and-probe procedure;
- binning in muon p_T and η ;
- shape hypotheses for the signal and the background in the fit model;
- other minor sources, such as the number of mass bins chosen, the selected mass range, and the kinematic selection criteria.

Uncertainties for all the sources are evaluated separately and are combined in quadrature.

Detector resolution effects, including the muon momentum scale correction, are major sources of systematic uncertainty in the dimuon channel. Both data and simulation are smeared by varying the muon momentum scale within its uncertainty. The difference between the cross

section values obtained with and without the smearing is assigned as a systematic uncertainty in each mass bin. In addition, contributions to the uncertainty relating to the unfolding of the detector resolution are:

- the statistical uncertainty in the response matrix due to the finite size of the MC sample;
- the systematic uncertainty in the response matrix arising from the differences in the MC modeling, as determined by comparing two different MC generators: POWHEG and MADGRAPH5_aMC@NLO.

In the dielectron channel, the dominant systematic uncertainty below the Z boson peak is the efficiency scale factor, as in the dimuon channel. Though the method to calculate this uncertainty is therefore similar, the possible sources are slightly different from those in the dimuon channel:

- statistical uncertainty associated with the tag-and-probe procedure;
- shape hypotheses for the signal and the background in the fit model;
- difference between the NLO and LO MC samples;
- different selection applied to the tag electron.

Detector resolution effects, including the electron energy scale and smearing corrections, are another significant systematic uncertainty in the dielectron channel. This uncertainty is determined with a method similar to that used in the dimuon channel, where the simulation is varied by the electron energy scale correction and smeared with the uncertainties. The difference between the central value and the smeared result for the cross section is assigned as the uncertainty. In addition, two other sources of systematic uncertainty in the detector resolution unfolding are considered for the dielectron channel: the statistical uncertainty in the response matrix and the difference between MC models. The uncertainty in the MC modeling is derived by comparing the results based on MADGRAPH5_aMC@NLO with those based on events reweighted with FEWZ package.

In both channels, the statistical uncertainty in the data sample, used for the background estimation, is one of the sources of systematic uncertainty; it is the dominant component in the higher mass region, above 200 GeV.

The difference between the background contributions estimated using control samples in data and the predictions from the MC simulation is one of the systematic uncertainty sources. In the cases where the background rates are estimated from MC simulation, the corresponding uncertainty in the predicted cross section is included as a systematic uncertainty although the contribution is negligible compared with other uncertainty components in the entire mass range.

The systematic uncertainty related to the acceptance is dominated by the theoretical component, which originates mainly from imperfect knowledge of nonperturbative effects, such as the PDFs. The PDF uncertainties are estimated using the NNLO version of FEWZ package and the FSR correction is applied in the calculation by using the dressed-lepton definition.

The difference between MADGRAPH5_aMC@NLO and FEWZ in the prediction of the DY differential cross section is assigned as an additional uncertainty in the acceptance. The uncertainty in the cross section due to the variation of the strong coupling constant, α_s , is estimated by varying the input value for the NNLO PDF used along with FEWZ.

The model-dependent FSR simulation is another source of uncertainty and it is evaluated by comparing the results from the PYTHIA and PHOTOS 3.56 [42] generators. The difference in the

cross section, after the FSR correction using dressed leptons, between the unfolding procedures of the PYTHIA and PHOTOS generators is assigned as a systematic uncertainty.

The uncertainty on the integrated luminosity measurement, based on pixel cluster counting in the silicon pixel detector, is 2.3% [43]. Figure 3 shows the estimated systematic uncertainties obtained in each mass bin; these are also summarised in Table 1 (2) for the dimuon (dielectron) channel. The uncertainty due to the acceptance and the PDFs originates from incomplete theoretical knowledge and is categorised separately from the other components, which are experimental in nature and are labelled “Total”.

8 Results

The differential cross section, in the full phase space, is estimated by extrapolation from the measurement within the fiducial region after the application of the set of corrections described in the previous sections. The detector fiducial volume is defined by the p_T and η requirements for the muons and electrons after FSR. The results are presented in Fig. 4 as a function of the dimuon and dielectron invariant mass covering the range 15 to 3000 GeV. They are compared with the NNLO theoretical predictions from FEWZ with NLO EW correction, as well as those from MADGRAPH5_aMC@NLO. Both predictions are calculated using the NNPDF3.0 PDF set. The ratios of the NLO and NNLO predictions to data are shown in the lower panels. The measurements are in good agreement, within uncertainties, with both theoretical predictions. Tables 3 and 4 show the summary of the results for the dimuon and dielectron channels, respectively.

In addition to the fully corrected total cross section, the fiducial cross section is also measured within the detector acceptance and without the FSR correction. Because of the fact that the acceptance correction, as shown in Fig. 2, is very large below the Z boson peak, the shape of the fiducial distribution is different in this mass region. Figure 5 shows the results in the dimuon and dielectron channels compared to the prediction from MADGRAPH5_aMC@NLO. Tables 5 and 6 present the summary of the fiducial cross section measurements (with no FSR correction applied) for the dimuon and dielectron channels, respectively. The results are in good agreement, within the uncertainties, with the theoretical prediction.

The differential cross section measurements obtained in the dimuon and dielectron channels in the full phase space are in good agreement with each other and therefore the results in the two channels are combined using the method described in Ref. [44]. The combined differential cross section in each bin is determined by the average of the two measurements weighted by the inverse of the squared total uncertainty. The uncertainty of the combined result is extracted from the diagonal elements of the covariance matrix of the combination, which is constructed using the covariance matrices of the measurements in the dimuon and dielectron channels. The uncertainties are considered to be uncorrelated between the two channels, with the exception of the integrated luminosity and the acceptance uncertainties. Systematic uncertainties are treated as additional uncorrelated uncertainties in the individual measurements, with the exception of the uncertainty from the efficiency scale factor. Statistical uncertainties are propagated to the covariance matrices of the measurements in the dimuon and dielectron channels before the combination.

The differential DY cross section for the full phase space, after the combination of the dimuon and dielectron channels, is presented in Fig. 6. The data point abscissas are computed according to Eq. (6) in Ref. [45]. Table 7 shows the summary of the combined results. Figure 7 shows a magnified ratio plot for the comparison of the theoretical prediction with experimental result

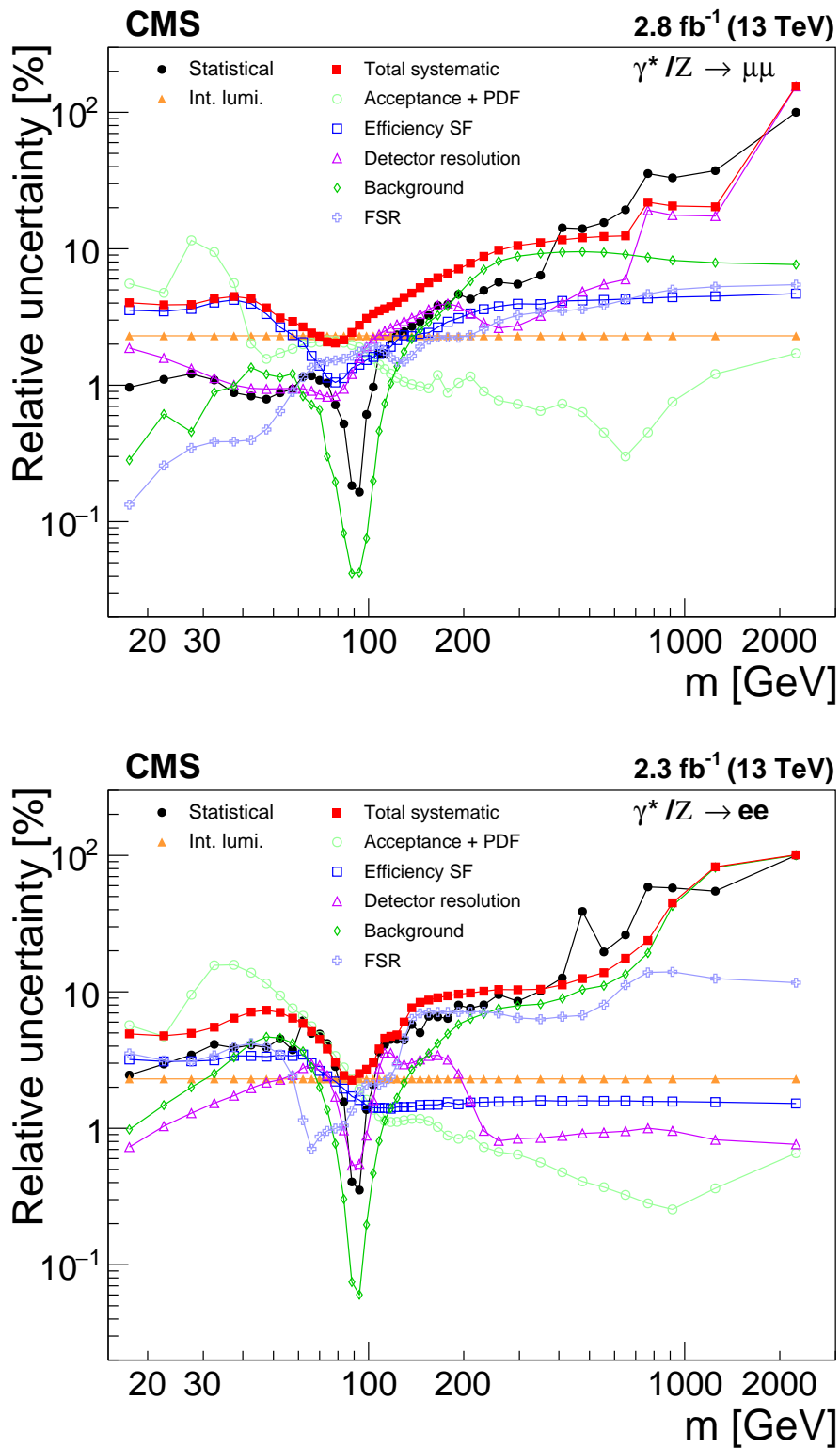


Figure 3: Summary of the systematic uncertainties on the differential cross section measurement $d\sigma/dm$ [pb/GeV] in the dimuon (upper) and dielectron (lower) channels. The “Total systematic” is a quadratic sum of all systematic uncertainty sources except for the “Acceptance + PDF”.

Table 1: Summary of the systematic uncertainties (%) for the $d\sigma/dm$ (pb/GeV) measurement in the dimuon channel. The column labelled “Total” corresponds to the quadratic sum of all the experimental sources, except for that Acceptance+PDF.

m (GeV)	Eff. (%)	Det. resol. (%)	Bkgr. est. (%)	FSR (%)	Total (%)	Acceptance+PDF (%)
15–20	3.5	1.9	0.28	0.13	4.0	5.6
20–25	3.5	1.6	0.61	0.26	3.9	4.8
25–30	3.6	1.3	0.45	0.35	3.9	12
30–35	4.0	1.1	0.89	0.38	4.3	9.5
35–40	4.2	1.0	0.98	0.39	4.5	5.6
40–45	4.0	0.95	1.3	0.40	4.3	2.0
45–50	3.3	0.94	1.2	0.47	3.7	1.6
50–55	2.7	0.94	1.1	0.65	3.1	1.7
55–60	2.3	0.95	1.2	0.89	2.9	1.8
60–64	2.1	0.94	0.83	1.1	2.7	2.0
64–68	1.6	0.91	0.72	1.3	2.4	2.0
68–72	1.4	0.86	0.66	1.5	2.3	2.1
72–76	1.1	0.82	0.30	1.5	2.1	2.1
76–81	1.0	0.83	0.20	1.5	2.0	2.1
81–86	1.1	0.94	0.082	1.6	2.1	2.0
86–91	1.3	1.2	0.042	1.6	2.4	2.0
91–96	1.4	1.6	0.042	1.8	2.8	1.9
96–101	1.5	1.9	0.075	1.9	3.1	1.7
101–106	1.6	2.2	0.20	1.9	3.3	1.6
106–110	1.7	2.4	0.46	1.9	3.5	1.4
110–115	1.8	2.5	0.73	1.8	3.6	1.3
115–120	1.9	2.6	1.0	1.6	3.8	1.2
120–126	2.1	2.8	1.4	1.5	4.0	1.1
126–133	2.3	2.9	1.8	1.5	4.4	1.1
133–141	2.3	3.1	2.2	1.6	4.7	1.0
141–150	2.4	3.3	2.6	1.9	5.2	0.98
150–160	2.4	3.6	2.9	2.2	5.6	0.95
160–171	2.7	3.9	3.3	2.2	6.1	1.2
171–185	2.9	4.0	3.8	2.2	6.6	0.88
185–200	3.1	3.8	4.7	2.2	7.1	1.0
200–220	3.4	3.3	5.8	2.3	7.8	1.2
220–243	3.6	2.9	7.0	2.6	8.8	0.90
243–273	3.8	2.6	8.1	2.9	9.8	0.77
273–320	3.9	2.7	8.8	3.3	11	0.73
320–380	3.9	3.2	9.2	3.4	11	0.65
380–440	4.1	4.0	9.5	3.5	12	0.73
440–510	4.2	4.9	9.5	3.6	12	0.64
510–600	4.2	5.5	9.4	3.8	12	0.45
600–700	4.3	6.0	9.1	4.2	12	0.30
700–830	4.3	19	8.7	4.7	22	0.45
830–1000	4.4	18	8.2	5.0	21	0.76
1000–1500	4.5	17	7.9	5.3	20	1.2
1500–3000	4.7	150	7.7	5.5	160	1.7

Table 2: Summary of the systematic uncertainties (%) for the $d\sigma/dm$ (pb/GeV) measurement in the dielectron channel. The column labelled “Total” corresponds to the quadratic sum of all the experimental sources, except for that Acceptance+PDF.

m (GeV)	Eff. (%)	Det. resol. (%)	Bkgr. est. (%)	FSR (%)	Total (%)	Acceptance+PDF (%)
15–20	3.2	0.73	0.98	3.5	4.9	5.7
20–25	3.1	1.0	1.5	3.1	4.8	4.7
25–30	3.1	1.3	2.0	3.1	5.0	9.5
30–35	3.2	1.5	2.5	3.4	5.5	16
35–40	3.4	1.7	3.3	3.9	6.4	16
40–45	3.4	2.0	4.2	4.2	7.1	14
45–50	3.4	2.2	4.7	4.0	7.3	12
50–55	3.4	2.3	4.6	3.5	7.1	9.4
55–60	3.4	2.5	4.2	2.4	6.4	7.6
60–64	3.5	2.8	3.7	1.1	5.9	6.7
64–68	3.0	3.0	2.8	0.71	5.1	5.6
68–72	2.6	2.9	2.0	0.87	4.5	4.7
72–76	2.4	2.4	1.4	0.96	3.8	4.0
76–81	2.2	1.7	0.77	1.0	3.1	3.4
81–86	2.0	0.97	0.30	1.0	2.4	2.8
86–91	1.7	0.53	0.075	1.3	2.2	2.3
91–96	1.6	0.55	0.060	1.9	2.5	1.9
96–101	1.5	0.88	0.20	2.1	2.7	1.6
101–106	1.4	1.6	0.47	2.1	3.0	1.4
106–110	1.4	2.8	0.81	2.1	3.8	1.2
110–115	1.4	3.6	1.1	2.2	4.6	1.1
115–120	1.4	3.6	1.4	2.4	4.7	1.1
120–126	1.4	3.1	1.7	2.9	4.8	1.1
126–133	1.4	2.9	2.1	4.6	6.0	1.1
133–141	1.4	3.0	2.7	6.3	7.6	1.2
141–150	1.5	3.2	3.1	7.0	8.4	1.2
150–160	1.5	3.4	3.5	7.0	8.7	1.1
160–171	1.5	3.4	4.2	7.1	9.1	1.0
171–185	1.6	3.2	4.9	7.1	9.4	0.88
185–200	1.5	2.5	5.8	7.1	9.6	0.84
200–220	1.5	1.6	6.3	7.1	9.8	0.89
220–243	1.6	0.96	6.9	7.2	10	0.73
243–273	1.6	0.81	7.5	6.9	10	0.67
273–320	1.6	0.84	7.9	6.4	10	0.64
320–380	1.6	0.85	8.1	6.3	10	0.56
380–440	1.6	0.88	9.0	6.6	11	0.48
440–510	1.6	0.92	10	6.7	13	0.41
510–600	1.6	0.93	11	8.0	14	0.37
600–700	1.6	0.95	13	11	18	0.32
700–830	1.6	1.0	19	14	24	0.28
830–1000	1.6	0.96	43	14	45	0.25
1000–1500	1.6	0.82	81	13	82	0.36
1500–3000	1.5	0.76	100	12	100	0.66

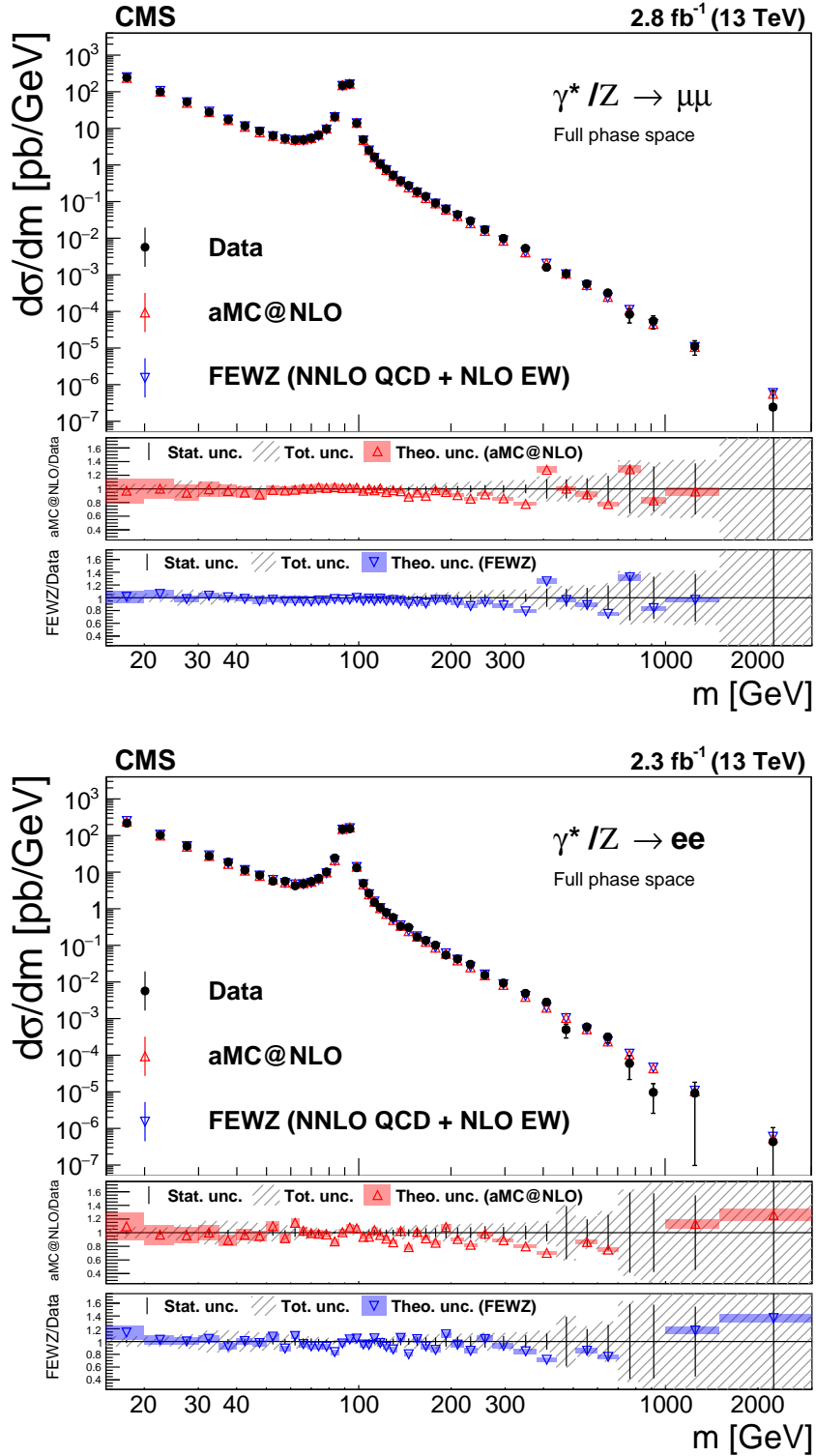


Figure 4: The differential cross section as a function of the dimuon (upper) and dielectron (lower) invariant mass, measured in the full phase space, with FSR correction applied. The spectra are compared with the NNLO theoretical prediction of FEWZ (blue) and the NLO prediction of MADGRAPH5_aMC@NLO (red). The NNPDF3.0 PDF set is used in both cases. In the middle and lower panels, the coloured bands denote the theoretical uncertainty and the hatched bands denote the total uncertainty, which is the combination of statistical, systematic, and integrated luminosity components.

Table 3: Summary of the measured values of $d\sigma/dm$ (pb/GeV) in the dimuon channel with the statistical (δ_{stat}), experimental (δ_{exp}) and theoretical (δ_{theo}) uncertainties, respectively. Here, δ_{tot} is the quadratic sum of the three components.

$m(\text{GeV})$	$\frac{d\sigma}{dm}$ (pb/GeV)	δ_{stat}	δ_{exp}	δ_{theo}	δ_{tot}
15–20	2.5×10^2	2.4×10^0	1.1×10^1	1.4×10^1	1.8×10^1
20–25	9.9×10^1	1.1×10^0	4.5×10^0	4.7×10^0	6.6×10^0
25–30	5.3×10^1	6.4×10^{-1}	2.4×10^0	6.1×10^0	6.6×10^0
30–35	2.8×10^1	3.0×10^{-1}	1.4×10^0	2.6×10^0	3.0×10^0
35–40	1.7×10^1	1.5×10^{-1}	8.7×10^{-1}	9.7×10^{-1}	1.3×10^0
40–45	1.2×10^1	9.7×10^{-2}	5.7×10^{-1}	2.3×10^{-1}	6.2×10^{-1}
45–50	8.5×10^0	6.7×10^{-2}	3.7×10^{-1}	1.3×10^{-1}	4.0×10^{-1}
50–55	6.3×10^0	5.5×10^{-2}	2.4×10^{-1}	1.1×10^{-1}	2.7×10^{-1}
55–60	5.3×10^0	5.0×10^{-2}	2.0×10^{-1}	9.8×10^{-2}	2.3×10^{-1}
60–64	4.9×10^0	5.6×10^{-2}	1.7×10^{-1}	9.7×10^{-2}	2.1×10^{-1}
64–68	4.9×10^0	5.8×10^{-2}	1.6×10^{-1}	1.0×10^{-1}	2.0×10^{-1}
68–72	5.4×10^0	5.9×10^{-2}	1.8×10^{-1}	1.1×10^{-1}	2.2×10^{-1}
72–76	6.5×10^0	6.8×10^{-2}	2.0×10^{-1}	1.4×10^{-1}	2.5×10^{-1}
76–81	9.7×10^0	7.0×10^{-2}	3.0×10^{-1}	2.0×10^{-1}	3.7×10^{-1}
81–86	2.1×10^1	1.1×10^{-1}	6.5×10^{-1}	4.2×10^{-1}	7.9×10^{-1}
86–91	1.5×10^2	2.7×10^{-1}	5.0×10^0	2.9×10^0	5.8×10^0
91–96	1.6×10^2	2.7×10^{-1}	5.9×10^0	3.1×10^0	6.6×10^0
96–101	1.4×10^1	8.5×10^{-2}	5.3×10^{-1}	2.4×10^{-1}	5.9×10^{-1}
101–106	4.9×10^0	4.8×10^{-2}	2.0×10^{-1}	7.6×10^{-2}	2.2×10^{-1}
106–110	2.5×10^0	4.3×10^{-2}	1.1×10^{-1}	3.6×10^{-2}	1.2×10^{-1}
110–115	1.7×10^0	2.8×10^{-2}	7.1×10^{-2}	2.2×10^{-2}	8.0×10^{-2}
115–120	1.1×10^0	2.3×10^{-2}	4.7×10^{-2}	1.3×10^{-2}	5.4×10^{-2}
120–126	7.6×10^{-1}	1.8×10^{-2}	3.5×10^{-2}	8.6×10^{-3}	4.1×10^{-2}
126–133	5.2×10^{-1}	1.3×10^{-2}	2.6×10^{-2}	5.5×10^{-3}	2.9×10^{-2}
133–141	3.7×10^{-1}	1.0×10^{-2}	1.9×10^{-2}	3.8×10^{-3}	2.2×10^{-2}
141–150	2.7×10^{-1}	8.0×10^{-3}	1.6×10^{-2}	2.7×10^{-3}	1.8×10^{-2}
150–160	1.9×10^{-1}	6.1×10^{-3}	1.1×10^{-2}	1.8×10^{-3}	1.3×10^{-2}
160–171	1.4×10^{-1}	5.3×10^{-3}	9.1×10^{-3}	1.6×10^{-3}	1.1×10^{-2}
171–185	9.1×10^{-2}	3.6×10^{-3}	6.4×10^{-3}	8.0×10^{-4}	7.3×10^{-3}
185–200	6.3×10^{-2}	2.9×10^{-3}	4.7×10^{-3}	6.5×10^{-4}	5.6×10^{-3}
200–220	4.4×10^{-2}	1.9×10^{-3}	3.6×10^{-3}	5.1×10^{-4}	4.1×10^{-3}
220–243	3.0×10^{-2}	1.5×10^{-3}	2.7×10^{-3}	2.7×10^{-4}	3.1×10^{-3}
243–273	1.7×10^{-2}	9.8×10^{-4}	1.7×10^{-3}	1.3×10^{-4}	2.0×10^{-3}
273–320	9.9×10^{-3}	5.4×10^{-4}	1.1×10^{-3}	7.2×10^{-5}	1.2×10^{-3}
320–380	5.3×10^{-3}	3.4×10^{-4}	6.0×10^{-4}	3.4×10^{-5}	6.9×10^{-4}
380–440	1.6×10^{-3}	2.3×10^{-4}	1.9×10^{-4}	1.2×10^{-5}	3.0×10^{-4}
440–510	1.1×10^{-3}	1.5×10^{-4}	1.3×10^{-4}	6.8×10^{-6}	2.0×10^{-4}
510–600	5.7×10^{-4}	8.9×10^{-5}	7.1×10^{-5}	2.6×10^{-6}	1.1×10^{-4}
600–700	3.2×10^{-4}	6.2×10^{-5}	4.0×10^{-5}	9.6×10^{-7}	7.4×10^{-5}
700–830	8.3×10^{-5}	3.0×10^{-5}	1.8×10^{-5}	3.8×10^{-7}	3.5×10^{-5}
830–1000	5.5×10^{-5}	1.8×10^{-5}	1.1×10^{-5}	4.1×10^{-7}	2.1×10^{-5}
1000–1500	1.1×10^{-5}	4.1×10^{-6}	2.3×10^{-6}	1.3×10^{-7}	4.7×10^{-6}
1500–3000	2.4×10^{-7}	2.4×10^{-7}	3.8×10^{-7}	4.2×10^{-9}	4.5×10^{-7}

Table 4: Summary of the measured values of $d\sigma/dm$ (pb/GeV) in the dielectron channel with the statistical (δ_{stat}), experimental (δ_{exp}) and theoretical (δ_{theo}) uncertainties, respectively. Here, δ_{tot} is the quadratic sum of the three components.

$m(\text{GeV})$	$\frac{d\sigma}{dm}$ (pb/GeV)	δ_{stat}	δ_{exp}	δ_{theo}	δ_{tot}
15–20	2.2×10^2	5.4×10^0	1.2×10^1	1.2×10^1	1.8×10^1
20–25	1.0×10^2	3.0×10^0	5.4×10^0	4.8×10^0	7.9×10^0
25–30	5.1×10^1	1.8×10^0	2.8×10^0	4.9×10^0	5.9×10^0
30–35	2.8×10^1	1.1×10^0	1.6×10^0	4.3×10^0	4.7×10^0
35–40	1.9×10^1	7.3×10^{-1}	1.3×10^0	3.0×10^0	3.3×10^0
40–45	1.1×10^1	4.6×10^{-1}	8.5×10^{-1}	1.6×10^0	1.8×10^0
45–50	8.2×10^0	3.2×10^{-1}	6.3×10^{-1}	9.5×10^{-1}	1.2×10^0
50–55	5.7×10^0	2.6×10^{-1}	4.2×10^{-1}	5.3×10^{-1}	7.3×10^{-1}
55–60	5.7×10^0	2.1×10^{-1}	3.9×10^{-1}	4.3×10^{-1}	6.1×10^{-1}
60–64	4.3×10^0	2.6×10^{-1}	2.7×10^{-1}	2.8×10^{-1}	4.7×10^{-1}
64–68	4.8×10^0	2.4×10^{-1}	2.7×10^{-1}	2.7×10^{-1}	4.5×10^{-1}
68–72	5.5×10^0	2.7×10^{-1}	2.8×10^{-1}	2.6×10^{-1}	4.7×10^{-1}
72–76	6.8×10^0	2.8×10^{-1}	3.0×10^{-1}	2.7×10^{-1}	4.9×10^{-1}
76–81	1.0×10^1	2.9×10^{-1}	3.8×10^{-1}	3.4×10^{-1}	5.9×10^{-1}
81–86	2.4×10^1	3.8×10^{-1}	8.2×10^{-1}	6.8×10^{-1}	1.1×10^0
86–91	1.5×10^2	6.0×10^{-1}	4.8×10^0	3.4×10^0	5.9×10^0
91–96	1.5×10^2	5.4×10^{-1}	5.2×10^0	3.0×10^0	6.1×10^0
96–101	1.3×10^1	1.8×10^{-1}	4.7×10^{-1}	2.1×10^{-1}	5.5×10^{-1}
101–106	4.9×10^0	1.0×10^{-1}	1.9×10^{-1}	6.7×10^{-2}	2.2×10^{-1}
106–110	2.6×10^0	9.5×10^{-2}	1.2×10^{-1}	3.2×10^{-2}	1.5×10^{-1}
110–115	1.5×10^0	6.2×10^{-2}	7.7×10^{-2}	1.7×10^{-2}	1.0×10^{-1}
115–120	1.1×10^0	4.8×10^{-2}	5.6×10^{-2}	1.2×10^{-2}	7.5×10^{-2}
120–126	7.9×10^{-1}	3.5×10^{-2}	4.2×10^{-2}	8.8×10^{-3}	5.6×10^{-2}
126–133	5.7×10^{-1}	2.5×10^{-2}	3.7×10^{-2}	6.6×10^{-3}	4.5×10^{-2}
133–141	3.3×10^{-1}	1.9×10^{-2}	2.7×10^{-2}	3.9×10^{-3}	3.3×10^{-2}
141–150	3.1×10^{-1}	1.6×10^{-2}	2.7×10^{-2}	3.6×10^{-3}	3.1×10^{-2}
150–160	1.7×10^{-1}	1.1×10^{-2}	1.5×10^{-2}	1.9×10^{-3}	1.9×10^{-2}
160–171	1.4×10^{-1}	8.9×10^{-3}	1.3×10^{-2}	1.4×10^{-3}	1.6×10^{-2}
171–185	1.0×10^{-1}	6.5×10^{-3}	9.8×10^{-3}	9.0×10^{-4}	1.2×10^{-2}
185–200	5.4×10^{-2}	4.4×10^{-3}	5.4×10^{-3}	4.6×10^{-4}	6.9×10^{-3}
200–220	4.3×10^{-2}	3.2×10^{-3}	4.3×10^{-3}	3.8×10^{-4}	5.4×10^{-3}
220–243	3.0×10^{-2}	2.4×10^{-3}	3.2×10^{-3}	2.2×10^{-4}	4.0×10^{-3}
243–273	1.5×10^{-2}	1.5×10^{-3}	1.6×10^{-3}	1.0×10^{-4}	2.2×10^{-3}
273–320	9.3×10^{-3}	7.9×10^{-4}	9.9×10^{-4}	6.0×10^{-5}	1.3×10^{-3}
320–380	4.9×10^{-3}	5.0×10^{-4}	5.2×10^{-4}	2.8×10^{-5}	7.2×10^{-4}
380–440	2.8×10^{-3}	3.6×10^{-4}	3.2×10^{-4}	1.3×10^{-5}	4.8×10^{-4}
440–510	5.0×10^{-4}	1.9×10^{-4}	6.4×10^{-5}	2.0×10^{-6}	2.0×10^{-4}
510–600	5.9×10^{-4}	1.2×10^{-4}	8.3×10^{-5}	2.2×10^{-6}	1.4×10^{-4}
600–700	3.2×10^{-4}	8.2×10^{-5}	5.6×10^{-5}	1.0×10^{-6}	1.0×10^{-4}
700–830	5.9×10^{-5}	3.5×10^{-5}	1.4×10^{-5}	1.7×10^{-7}	3.8×10^{-5}
830–1000	9.6×10^{-6}	5.6×10^{-6}	4.3×10^{-6}	2.5×10^{-8}	7.1×10^{-6}
1000–1500	9.1×10^{-6}	5.0×10^{-6}	7.5×10^{-6}	3.3×10^{-8}	9.0×10^{-6}
1500–3000	4.3×10^{-7}	4.3×10^{-7}	4.4×10^{-7}	2.8×10^{-9}	6.2×10^{-7}

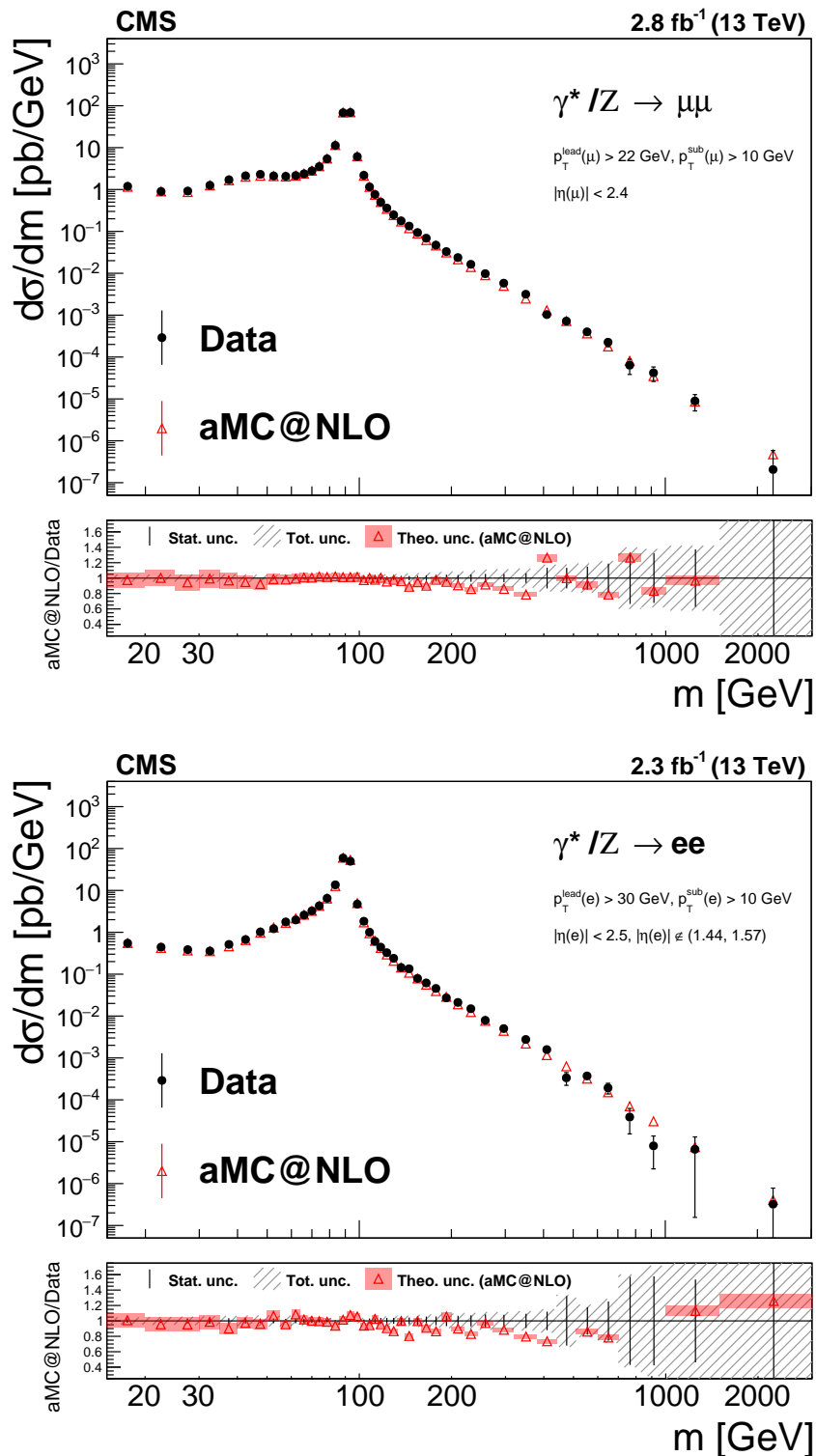


Figure 5: Comparison between the measured fiducial cross section (with no FSR correction applied) and the NLO theoretical prediction of MADGRAPH5_aMC@NLO with NNPDF 3.0 in the dimuon (upper) and dielectron (lower) channels. In the bottom panels, the red band represents the theoretical uncertainty and the hatched band represents the total uncertainty, which is the combination of the statistical, systematic, and integrated luminosity components.

Table 5: Summary of the measured values of fiducial $d\sigma/dm$ (pb/GeV) (with no FSR correction applied) in the dimuon channel with the statistical (δ_{stat}) and experimental (δ_{exp}) uncertainties shown separately. Here, δ_{tot} is the quadratic sum of the two components.

$m(\text{GeV})$	$\frac{d\sigma}{dm}$ (pb/GeV)	δ_{stat}	δ_{exp}	δ_{tot}
15–20	1.2×10^0	1.1×10^{-2}	5.5×10^{-2}	5.6×10^{-2}
20–25	9.0×10^{-1}	9.8×10^{-3}	4.0×10^{-2}	4.2×10^{-2}
25–30	9.2×10^{-1}	1.1×10^{-2}	4.2×10^{-2}	4.3×10^{-2}
30–35	1.3×10^0	1.3×10^{-2}	6.1×10^{-2}	6.3×10^{-2}
35–40	1.7×10^0	1.5×10^{-2}	8.6×10^{-2}	8.7×10^{-2}
40–45	2.1×10^0	1.7×10^{-2}	1.0×10^{-1}	1.0×10^{-1}
45–50	2.3×10^0	1.7×10^{-2}	1.0×10^{-1}	1.0×10^{-1}
50–55	2.1×10^0	1.7×10^{-2}	8.1×10^{-2}	8.2×10^{-2}
55–60	2.1×10^0	1.7×10^{-2}	7.5×10^{-2}	7.7×10^{-2}
60–64	2.2×10^0	2.0×10^{-2}	7.2×10^{-2}	7.5×10^{-2}
64–68	2.4×10^0	2.2×10^{-2}	7.2×10^{-2}	7.6×10^{-2}
68–72	2.8×10^0	2.3×10^{-2}	8.1×10^{-2}	8.4×10^{-2}
72–76	3.5×10^0	2.7×10^{-2}	9.6×10^{-2}	9.9×10^{-2}
76–81	5.4×10^0	2.8×10^{-2}	1.4×10^{-1}	1.5×10^{-1}
81–86	1.1×10^1	4.5×10^{-2}	3.1×10^{-1}	3.1×10^{-1}
86–91	6.8×10^1	1.1×10^{-1}	2.0×10^0	2.0×10^0
91–96	6.9×10^1	1.1×10^{-1}	2.2×10^0	2.2×10^0
96–101	6.1×10^0	3.6×10^{-2}	2.1×10^{-1}	2.1×10^{-1}
101–106	2.2×10^0	2.0×10^{-2}	7.8×10^{-2}	8.1×10^{-2}
106–110	1.2×10^0	1.9×10^{-2}	4.3×10^{-2}	4.7×10^{-2}
110–115	7.6×10^{-1}	1.2×10^{-2}	3.0×10^{-2}	3.2×10^{-2}
115–120	5.0×10^{-1}	1.0×10^{-2}	2.1×10^{-2}	2.3×10^{-2}
120–126	3.6×10^{-1}	7.9×10^{-3}	1.6×10^{-2}	1.8×10^{-2}
126–133	2.5×10^{-1}	5.8×10^{-3}	1.2×10^{-2}	1.3×10^{-2}
133–141	1.8×10^{-1}	4.5×10^{-3}	8.9×10^{-3}	1.0×10^{-2}
141–150	1.3×10^{-1}	3.7×10^{-3}	7.2×10^{-3}	8.1×10^{-3}
150–160	9.4×10^{-2}	2.9×10^{-3}	5.3×10^{-3}	6.1×10^{-3}
160–171	6.9×10^{-2}	2.5×10^{-3}	4.2×10^{-3}	4.9×10^{-3}
171–185	4.7×10^{-2}	1.7×10^{-3}	3.1×10^{-3}	3.6×10^{-3}
185–200	3.3×10^{-2}	1.4×10^{-3}	2.4×10^{-3}	2.8×10^{-3}
200–220	2.4×10^{-2}	9.7×10^{-4}	1.9×10^{-3}	2.1×10^{-3}
220–243	1.6×10^{-2}	7.7×10^{-4}	1.4×10^{-3}	1.6×10^{-3}
243–273	9.8×10^{-3}	5.3×10^{-4}	9.4×10^{-4}	1.1×10^{-3}
273–320	5.8×10^{-3}	3.1×10^{-4}	6.0×10^{-4}	6.7×10^{-4}
320–380	3.2×10^{-3}	2.0×10^{-4}	3.4×10^{-4}	3.9×10^{-4}
380–440	1.0×10^{-3}	1.4×10^{-4}	1.2×10^{-4}	1.8×10^{-4}
440–510	7.2×10^{-4}	9.6×10^{-5}	8.5×10^{-5}	1.3×10^{-4}
510–600	4.0×10^{-4}	6.0×10^{-5}	4.8×10^{-5}	7.6×10^{-5}
600–700	2.3×10^{-4}	4.3×10^{-5}	2.7×10^{-5}	5.0×10^{-5}
700–830	6.4×10^{-5}	2.1×10^{-5}	1.4×10^{-5}	2.5×10^{-5}
830–1000	4.2×10^{-5}	1.4×10^{-5}	8.4×10^{-6}	1.6×10^{-5}
1000–1500	8.9×10^{-6}	3.3×10^{-6}	1.8×10^{-6}	3.8×10^{-6}
1500–3000	2.1×10^{-7}	2.1×10^{-7}	3.2×10^{-7}	3.8×10^{-7}

Table 6: Summary of the measured values of fiducial $d\sigma/dm$ (pb/GeV) (with no FSR correction applied) in the dielectron channel with the statistical (δ_{stat}) and experimental (δ_{exp}) uncertainties shown separately. Here, δ_{tot} is the quadratic sum of the two components.

$m(\text{GeV})$	$\frac{d\sigma}{dm}$ (pb/GeV)	δ_{stat}	δ_{exp}	δ_{tot}
15–20	5.5×10^{-1}	1.3×10^{-2}	2.3×10^{-2}	2.6×10^{-2}
20–25	4.4×10^{-1}	1.2×10^{-2}	1.9×10^{-2}	2.3×10^{-2}
25–30	3.9×10^{-1}	1.2×10^{-2}	1.7×10^{-2}	2.1×10^{-2}
30–35	3.6×10^{-1}	1.3×10^{-2}	1.7×10^{-2}	2.2×10^{-2}
35–40	5.1×10^{-1}	1.8×10^{-2}	2.9×10^{-2}	3.4×10^{-2}
40–45	6.7×10^{-1}	2.3×10^{-2}	4.1×10^{-2}	4.7×10^{-2}
45–50	1.0×10^0	3.1×10^{-2}	6.7×10^{-2}	7.4×10^{-2}
50–55	1.2×10^0	3.8×10^{-2}	8.0×10^{-2}	8.9×10^{-2}
55–60	1.8×10^0	4.3×10^{-2}	1.1×10^{-1}	1.2×10^{-1}
60–64	2.0×10^0	6.0×10^{-2}	1.2×10^{-1}	1.4×10^{-1}
64–68	2.6×10^0	6.7×10^{-2}	1.4×10^{-1}	1.6×10^{-1}
68–72	3.2×10^0	7.6×10^{-2}	1.6×10^{-1}	1.8×10^{-1}
72–76	4.3×10^0	8.3×10^{-2}	1.9×10^{-1}	2.0×10^{-1}
76–81	6.5×10^0	8.7×10^{-2}	2.4×10^{-1}	2.5×10^{-1}
81–86	1.4×10^1	1.2×10^{-1}	4.3×10^{-1}	4.5×10^{-1}
86–91	5.9×10^1	1.9×10^{-1}	1.7×10^0	1.7×10^0
91–96	5.0×10^1	1.7×10^{-1}	1.4×10^0	1.4×10^0
96–101	4.7×10^0	5.9×10^{-2}	1.4×10^{-1}	1.5×10^{-1}
101–106	1.8×10^0	3.4×10^{-2}	5.8×10^{-2}	6.7×10^{-2}
106–110	1.0×10^0	3.1×10^{-2}	4.0×10^{-2}	5.1×10^{-2}
110–115	6.1×10^{-1}	2.1×10^{-2}	2.8×10^{-2}	3.5×10^{-2}
115–120	4.4×10^{-1}	1.7×10^{-2}	2.1×10^{-2}	2.7×10^{-2}
120–126	3.3×10^{-1}	1.3×10^{-2}	1.5×10^{-2}	1.9×10^{-2}
126–133	2.4×10^{-1}	9.3×10^{-3}	1.1×10^{-2}	1.4×10^{-2}
133–141	1.4×10^{-1}	7.0×10^{-3}	7.0×10^{-3}	9.9×10^{-3}
141–150	1.3×10^{-1}	5.9×10^{-3}	7.0×10^{-3}	9.2×10^{-3}
150–160	7.9×10^{-2}	4.4×10^{-3}	4.4×10^{-3}	6.3×10^{-3}
160–171	6.2×10^{-2}	3.5×10^{-3}	3.7×10^{-3}	5.1×10^{-3}
171–185	4.6×10^{-2}	2.6×10^{-3}	3.0×10^{-3}	3.9×10^{-3}
185–200	2.7×10^{-2}	1.9×10^{-3}	1.9×10^{-3}	2.6×10^{-3}
200–220	2.1×10^{-2}	1.4×10^{-3}	1.5×10^{-3}	2.1×10^{-3}
220–243	1.5×10^{-2}	1.1×10^{-3}	1.1×10^{-3}	1.6×10^{-3}
243–273	7.9×10^{-3}	6.7×10^{-4}	6.4×10^{-4}	9.3×10^{-4}
273–320	5.0×10^{-3}	4.0×10^{-4}	4.2×10^{-4}	5.8×10^{-4}
320–380	2.8×10^{-3}	2.6×10^{-4}	2.4×10^{-4}	3.5×10^{-4}
380–440	1.6×10^{-3}	1.9×10^{-4}	1.5×10^{-4}	2.4×10^{-4}
440–510	3.4×10^{-4}	1.1×10^{-4}	3.6×10^{-5}	1.1×10^{-4}
510–600	3.7×10^{-4}	6.6×10^{-5}	4.3×10^{-5}	7.9×10^{-5}
600–700	1.9×10^{-4}	4.9×10^{-5}	2.7×10^{-5}	5.5×10^{-5}
700–830	3.9×10^{-5}	2.2×10^{-5}	7.6×10^{-6}	2.3×10^{-5}
830–1000	8.0×10^{-6}	4.6×10^{-6}	3.4×10^{-6}	5.7×10^{-6}
1000–1500	6.6×10^{-6}	3.5×10^{-6}	5.4×10^{-6}	6.4×10^{-6}
1500–3000	3.2×10^{-7}	3.2×10^{-7}	3.2×10^{-7}	4.6×10^{-7}

in two mass ranges, $15 < m < 200 \text{ GeV}$ and $200 < m < 3000 \text{ GeV}$. In the bottom plot of the figure, an additional theoretical prediction, containing the photon-induced contribution calculated using FEWZ with the LUXqed PDF set, is included. There is a sizable effect from this contribution in the high-mass region. The level of agreement between data and theory is very good as indicated by the p -value of 0.49 except for $830 < m < 1000 \text{ GeV}$, determined from the χ^2 comparison between the combined result and NNLO prediction.

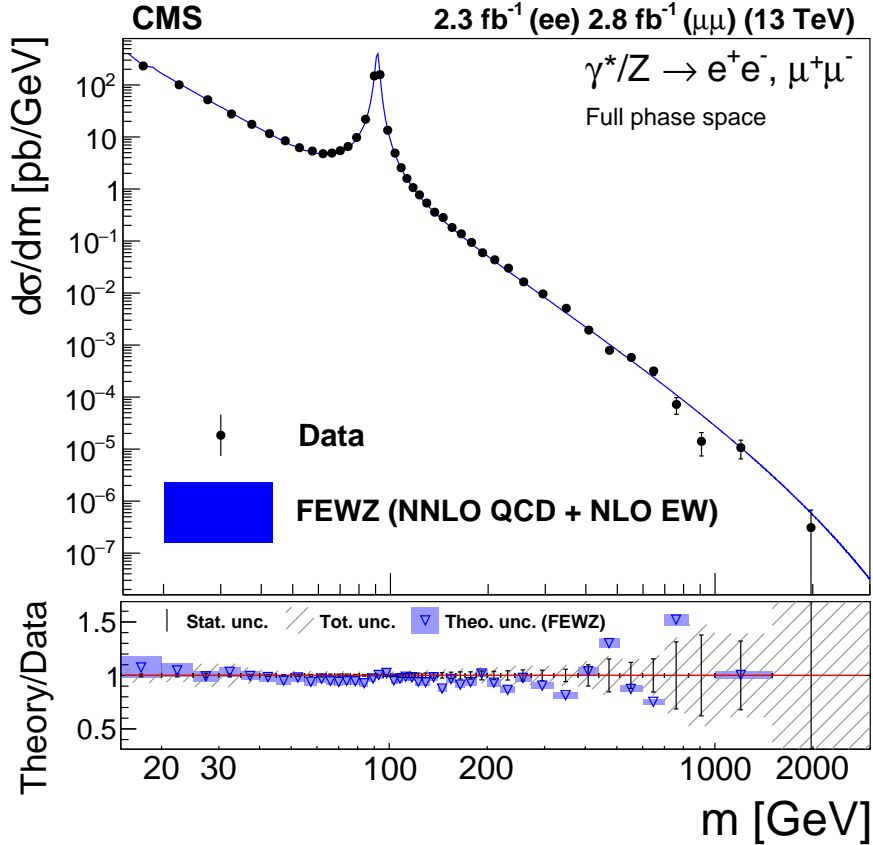


Figure 6: The differential DY cross section measured for the combination of the two channels and as predicted by the NNLO theoretical calculation of FEWZ with NNPDF 3.0 in the full phase space. The ratio between the data and the theoretical prediction is presented in the bottom panel. The coloured boxes represent the theoretical uncertainties.

9 Summary

This paper presents measurements of the total and fiducial Drell–Yan differential cross sections $d\sigma/dm$ in the dimuon and the dielectron channels as well as their combination, in the dilepton invariant mass range $15 < m < 3000 \text{ GeV}$, using data collected by the CMS experiment, in proton-proton collisions at a centre-of-mass energy of 13 TeV , corresponding to an integrated luminosity of up to 2.8 fb^{-1} . The data are corrected for detector resolution effects, the differences in the efficiency between data and Monte Carlo simulation, and the acceptance. Additionally the final-state photon radiation effects, which are most pronounced below the Z boson peak, are included. The results are in good agreement with the theoretical predictions of the standard model.

Table 7: Summary of the combined values of $d\sigma/dm$ (pb/GeV) using the results from both the dimuon and dielectron channels. Here, δ_{tot} is the quadratic sum of the statistical, experimental and theoretical uncertainties.

$m(\text{GeV})$	$\frac{d\sigma}{dm}$ (pb/GeV)	δ_{tot}
15–20	2.3×10^2	1.6×10^1
20–25	1.0×10^2	6.3×10^0
25–30	5.2×10^1	5.7×10^0
30–35	2.8×10^1	3.0×10^0
35–40	1.8×10^1	1.3×10^0
40–45	1.2×10^1	6.1×10^{-1}
45–50	8.5×10^0	3.9×10^{-1}
50–55	6.2×10^0	2.7×10^{-1}
55–60	5.4×10^0	2.3×10^{-1}
60–64	4.8×10^0	2.0×10^{-1}
64–68	4.9×10^0	2.0×10^{-1}
68–72	5.4×10^0	2.2×10^{-1}
72–76	6.6×10^0	2.6×10^{-1}
76–81	9.8×10^0	3.7×10^{-1}
81–86	2.2×10^1	7.9×10^{-1}
86–91	1.5×10^2	5.2×10^0
91–96	1.6×10^2	5.6×10^0
96–101	1.3×10^1	4.8×10^{-1}
101–106	4.9×10^0	1.8×10^{-1}
106–110	2.6×10^0	1.1×10^{-1}
110–115	1.6×10^0	6.8×10^{-2}
115–120	1.1×10^0	4.7×10^{-2}
120–126	7.7×10^{-1}	3.5×10^{-2}
126–133	5.4×10^{-1}	2.6×10^{-2}
133–141	3.6×10^{-1}	1.9×10^{-2}
141–150	2.8×10^{-1}	1.6×10^{-2}
150–160	1.8×10^{-1}	1.1×10^{-2}
160–171	1.4×10^{-1}	9.1×10^{-3}
171–185	9.4×10^{-2}	6.4×10^{-3}
185–200	6.0×10^{-2}	4.5×10^{-3}
200–220	4.4×10^{-2}	3.3×10^{-3}
220–243	3.0×10^{-2}	2.5×10^{-3}
243–273	1.6×10^{-2}	1.5×10^{-3}
273–320	9.6×10^{-3}	8.9×10^{-4}
320–380	5.1×10^{-3}	5.0×10^{-4}
380–440	1.9×10^{-3}	2.5×10^{-4}
440–510	7.9×10^{-4}	1.4×10^{-4}
510–600	5.8×10^{-4}	8.9×10^{-5}
600–700	3.2×10^{-4}	6.0×10^{-5}
700–830	7.2×10^{-5}	2.6×10^{-5}
830–1000	1.4×10^{-5}	6.7×10^{-6}
1000–1500	1.1×10^{-5}	4.2×10^{-6}
1500–3000	3.1×10^{-7}	3.6×10^{-7}

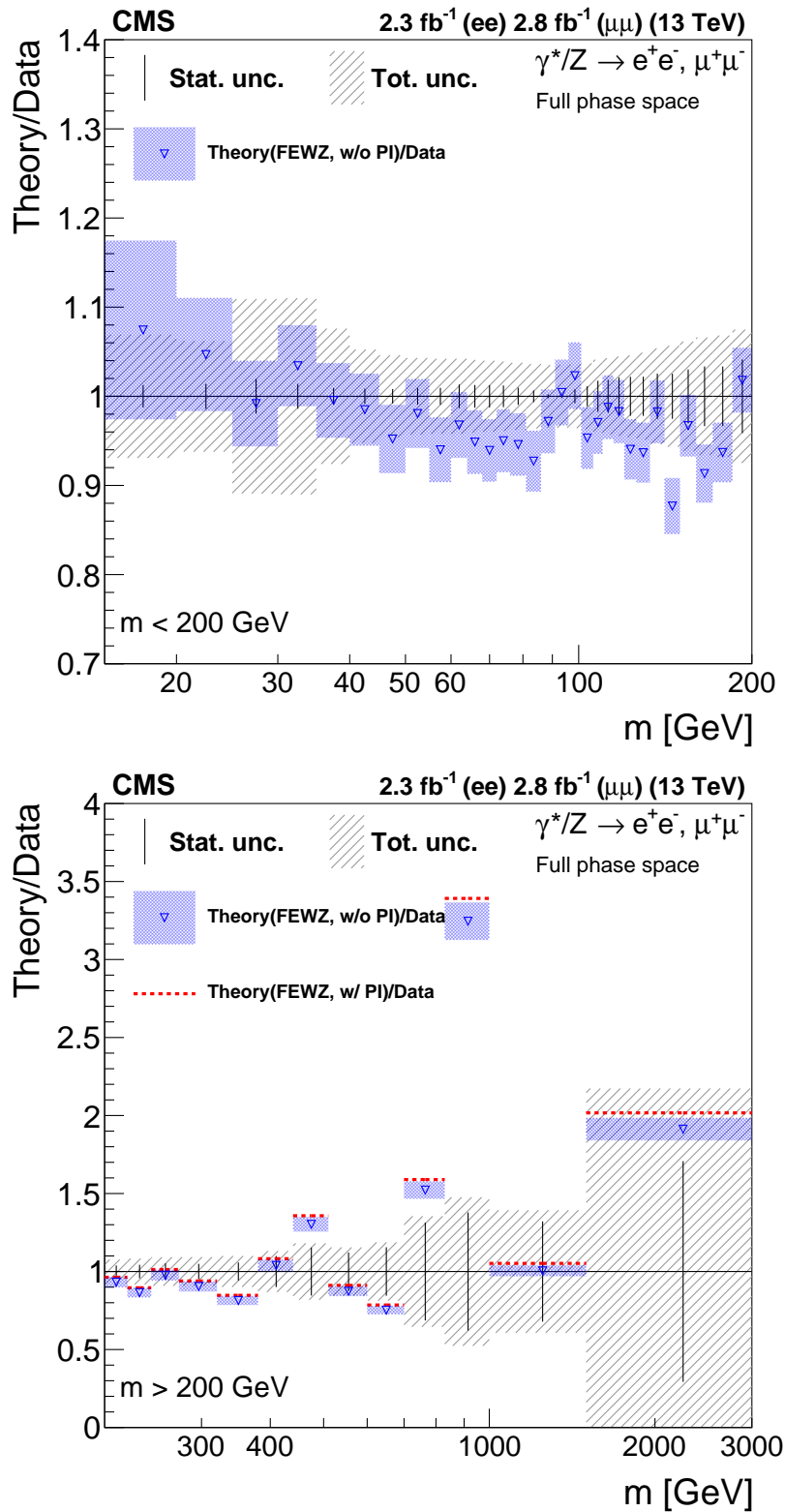


Figure 7: Magnified view of the ratio of the NNLO theoretical prediction of FEWZ with NNPDF 3.0 to data for the combined differential cross sections in two different mass ranges: $m < 200$ GeV (top) and $m > 200$ GeV (bottom). The blue bands represent the theoretical uncertainty on the ratio. The bottom plot also shows the ratio with the photon-induced contribution (red dashed lines), which has a sizable effect in the high-mass region.

Acknowledgments

We congratulate our colleagues in the CERN accelerator departments for the excellent performance of the LHC and thank the technical and administrative staffs at CERN and at other CMS institutes for their contributions to the success of the CMS effort. In addition, we gratefully acknowledge the computing centres and personnel of the Worldwide LHC Computing Grid for delivering so effectively the computing infrastructure essential to our analyses. Finally, we acknowledge the enduring support for the construction and operation of the LHC and the CMS detector provided by the following funding agencies: BMBWF and FWF (Austria); FNRS and FWO (Belgium); CNPq, CAPES, FAPERJ, FAPERGS, and FAPESP (Brazil); MES (Bulgaria); CERN; CAS, MoST, and NSFC (China); COLCIENCIAS (Colombia); MSES and CSF (Croatia); RPF (Cyprus); SENESCYT (Ecuador); MoER, ERC IUT, and ERDF (Estonia); Academy of Finland, MEC, and HIP (Finland); CEA and CNRS/IN2P3 (France); BMBF, DFG, and HGF (Germany); GSRT (Greece); NKFI (Hungary); DAE and DST (India); IPM (Iran); SFI (Ireland); INFN (Italy); MSIP and NRF (Republic of Korea); MES (Latvia); LAS (Lithuania); MOE and UM (Malaysia); BUAP, CINVESTAV, CONACYT, LNS, SEP, and UASLP-FAI (Mexico); MOS (Montenegro); MBIE (New Zealand); PAEC (Pakistan); MSHE and NSC (Poland); FCT (Portugal); JINR (Dubna); MON, RosAtom, RAS, RFBR, and NRC KI (Russia); MESTD (Serbia); SEIDI, CPAN, PCTI, and FEDER (Spain); MOSTR (Sri Lanka); Swiss Funding Agencies (Switzerland); MST (Taipei); ThEPCenter, IPST, STAR, and NSTDA (Thailand); TUBITAK and TAEK (Turkey); NASU and SFFR (Ukraine); STFC (United Kingdom); DOE and NSF (USA).

Individuals have received support from the Marie-Curie programme and the European Research Council and Horizon 2020 Grant, contract No. 675440 (European Union); the Leventis Foundation; the A. P. Sloan Foundation; the Alexander von Humboldt Foundation; the Belgian Federal Science Policy Office; the Fonds pour la Formation à la Recherche dans l'Industrie et dans l'Agriculture (FRIA-Belgium); the Agentschap voor Innovatie door Wetenschap en Technologie (IWT-Belgium); the F.R.S.-FNRS and FWO (Belgium) under the "Excellence of Science - EOS" - be.h project n. 30820817; the Ministry of Education, Youth and Sports (MEYS) of the Czech Republic; the Lendület ("Momentum") Programme and the János Bolyai Research Scholarship of the Hungarian Academy of Sciences, the New National Excellence Program ÚNKP, the NKFI research grants 123842, 123959, 124845, 124850 and 125105 (Hungary); the Council of Science and Industrial Research, India; the HOMING PLUS programme of the Foundation for Polish Science, cofinanced from European Union, Regional Development Fund, the Mobility Plus programme of the Ministry of Science and Higher Education, the National Science Center (Poland), contracts Harmonia 2014/14/M/ST2/00428, Opus 2014/13/B/ST2/02543, 2014/15/B/ST2/03998, and 2015/19/B/ST2/02861, Sonata-bis 2012/07/E/ST2/01406; the National Priorities Research Program by Qatar National Research Fund; the Programa Estatal de Fomento de la Investigación Científica y Técnica de Excelencia María de Maeztu, grant MDM-2015-0509 and the Programa Severo Ochoa del Principado de Asturias; the Thalís and Aristeia programmes cofinanced by EU-ESF and the Greek NSRF; the Rachadapisek Sompot Fund for Postdoctoral Fellowship, Chulalongkorn University and the Chulalongkorn Academic into Its 2nd Century Project Advancement Project (Thailand); the Welch Foundation, contract C-1845; and the Weston Havens Foundation (USA).

References

- [1] R. Hamberg, W. L. van Neerven, and T. Matsuura, "A complete calculation of the order α_s^2 correction to the Drell–Yan k-factor", *Nucl. Phys. B* **359** (1991) 343,

doi:10.1016/0550-3213(91)90064-5.
[Erratum:doi:10.1016/S0550-3213(02)00814-3].

- [2] S. Catani et al., “Vector boson production at hadron colliders: A fully exclusive QCD calculation at next-to-next-to-leading order”, *Phys. Rev. Lett.* **103** (2009) 082001, doi:10.1103/PhysRevLett.103.082001, arXiv:0903.2120.
- [3] S. Catani and M. Grazzini, “Next-to-next-to-leading-order subtraction formalism in hadron collisions and its application to Higgs-boson production at the Large Hadron Collider”, *Phys. Rev. Lett.* **98** (2007) 222002, doi:10.1103/PhysRevLett.98.222002, arXiv:hep-ph/0703012.
- [4] K. Melnikov and F. Petriello, “Electroweak gauge boson production at hadron colliders through $O(\alpha_s^2)$ ”, *Phys. Rev. D* **74** (2006) 114017, doi:10.1103/PhysRevD.74.114017, arXiv:hep-ph/0609070.
- [5] ATLAS Collaboration, “Measurement of the high-mass Drell–Yan differential cross-section in pp collisions at $\sqrt{s} = 7$ TeV with the ATLAS detector”, *Phys. Lett. B* **725** (2013) 223, doi:10.1016/j.physletb.2013.07.049, arXiv:1305.4192.
- [6] ATLAS Collaboration, “Measurement of the low-mass Drell–Yan differential cross section at $\sqrt{s} = 7$ TeV using the ATLAS detector”, *JHEP* **06** (2014) 112, doi:10.1007/JHEP06(2014)112, arXiv:1404.1212.
- [7] ATLAS Collaboration, “Measurement of the double-differential high-mass Drell–Yan cross section in pp collisions at $\sqrt{s} = 8$ TeV with the ATLAS detector”, *JHEP* **08** (2016) 009, doi:10.1007/JHEP08(2016)009, arXiv:1606.01736.
- [8] CMS Collaboration, “Measurement of the Drell–Yan cross section in pp collisions at $\sqrt{s} = 7$ TeV”, *JHEP* **10** (2011) 007, doi:10.1007/JHEP10(2011)007, arXiv:1108.0566.
- [9] CMS Collaboration, “Measurement of the differential and double-differential Drell–Yan cross sections in proton-proton collisions at $\sqrt{s} = 7$ TeV”, *JHEP* **12** (2013) 030, doi:10.1007/JHEP12(2013)030, arXiv:1310.7291.
- [10] CMS Collaboration, “Measurement of differential and double-differential Drell–Yan cross sections in proton-proton collisions at $\sqrt{s} = 8$ TeV”, *Eur. Phys. J. C* **75** (2015) 147, doi:10.1140/epjc/s10052-015-3364-2, arXiv:1412.1115.
- [11] ATLAS Collaboration, “Measurement of W^\pm and Z-boson production cross sections in pp collisions at $\sqrt{s} = 13$ TeV with the ATLAS detector”, *Phys. Lett. B* **759** (2016) 601, doi:10.1016/j.physletb.2016.06.023, arXiv:1603.09222.
- [12] CMS Collaboration, “Performance of electron reconstruction and selection with the CMS detector in proton-proton collisions at $\sqrt{s} = 8$ TeV”, *JINST* **10** (2015) P06005, doi:10.1088/1748-0221/10/06/P06005, arXiv:1502.02701.
- [13] CMS Collaboration, “Performance of the CMS muon detector and muon reconstruction with proton-proton collisions at $\sqrt{s} = 13$ TeV”, *JINST* **13** (2018) P06015, doi:10.1088/1748-0221/13/06/P06015, arXiv:1804.04528.
- [14] CMS Collaboration, “The CMS trigger system”, *JINST* **12** (2017) P01020, doi:10.1088/1748-0221/12/01/P01020, arXiv:1609.02366.

- [15] CMS Collaboration, “The CMS experiment at the CERN LHC”, *JINST* **3** (2008) S08004, doi:10.1088/1748-0221/3/08/S08004.
- [16] J. Alwall et al., “The automated computation of tree-level and next-to-leading order differential cross sections, and their matching to parton shower simulations”, *JHEP* **07** (2014) 079, doi:10.1007/JHEP07(2014)079, arXiv:1405.0301.
- [17] P. Nason, “A new method for combining NLO QCD with shower Monte Carlo algorithms”, *JHEP* **11** (2004) 040, doi:10.1088/1126-6708/2004/11/040, arXiv:hep-ph/0409146.
- [18] S. Frixione, P. Nason, and C. Oleari, “Matching NLO QCD computations with parton shower simulations: the POWHEG method”, *JHEP* **11** (2007) 070, doi:10.1088/1126-6708/2007/11/070, arXiv:0709.2092.
- [19] S. Alioli, P. Nason, C. Oleari, and E. Re, “A general framework for implementing NLO calculations in shower Monte Carlo programs: the POWHEG BOX”, *JHEP* **06** (2010) 043, doi:10.1007/JHEP06(2010)043, arXiv:1002.2581.
- [20] S. Frixione, P. Nason, and G. Ridolfi, “A positive-weight next-to-leading-order Monte Carlo for heavy flavour hadroproduction”, *JHEP* **09** (2007) 126, doi:10.1088/1126-6708/2007/09/126, arXiv:0707.3088.
- [21] E. Re, “Single-top Wt -channel production matched with parton showers using the POWHEG method”, *Eur. Phys. J. C* **71** (2011) 1547, doi:10.1140/epjc/s10052-011-1547-z, arXiv:1009.2450.
- [22] T. Sjöstrand et al., “An introduction to PYTHIA 8.2”, *Comput. Phys. Commun.* **191** (2015) 159, doi:10.1016/j.cpc.2015.01.024, arXiv:1410.3012.
- [23] NNPDF Collaboration, “A first unbiased global NLO determination of parton distributions and their uncertainties”, *Nucl. Phys. B* **838** (2010) 136, doi:10.1016/j.nuclphysb.2010.05.008, arXiv:1002.4407.
- [24] NNPDF Collaboration, “Parton distributions for the LHC Run II”, *JHEP* **04** (2015) 040, doi:10.1007/JHEP04(2015)040, arXiv:1410.8849.
- [25] CMS Collaboration, “Event generator tunes obtained from underlying event and multiparton scattering measurements”, *Eur. Phys. J. C* **76** (2016) 155, doi:10.1140/epjc/s10052-016-3988-x, arXiv:1512.00815.
- [26] R. Frederix and S. Frixione, “Merging meets matching in MC@NLO”, *JHEP* **12** (2012) 061, doi:10.1007/JHEP12(2012)061, arXiv:1209.6215.
- [27] M. Czakon and A. Mitov, “Top++: A program for the calculation of the top-pair cross-section at hadron colliders”, *Comput. Phys. Commun.* **185** (2014) 2930, doi:10.1016/j.cpc.2014.06.021, arXiv:1112.5675.
- [28] J. M. Campbell, R. K. Ellis, and C. Williams, “Vector boson pair production at the LHC”, *JHEP* **07** (2011) 018, doi:10.1007/JHEP07(2011)018, arXiv:1105.0020.
- [29] T. Melia, P. Nason, R. Rötsch, and G. Zanderighi, “ W^+W^- , WZ and ZZ production in the POWHEG BOX”, *JHEP* **11** (2011) 078, doi:10.1007/JHEP11(2011)078, arXiv:1107.5051.

-
- [30] GEANT4 Collaboration, “GEANT4 — a simulation toolkit”, *Nucl. Instrum. Meth. A* **506** (2003) 250, doi:10.1016/S0168-9002(03)01368-8.
- [31] CMS Collaboration, “Particle-flow reconstruction and global event description with the CMS detector”, *JINST* **12** (2017) P10003, doi:10.1088/1748-0221/12/10/P10003, arXiv:1706.04965.
- [32] CMS Collaboration, “Energy calibration and resolution of the CMS electromagnetic calorimeter in pp collisions at $\sqrt{s} = 7$ TeV”, *JINST* **8** (2013) P09009, doi:10.1088/1748-0221/8/09/P09009, arXiv:1306.2016.
- [33] A. Bodek et al., “Extracting muon momentum scale corrections for hadron collider experiments”, *Eur. Phys. J. C* **72** (2012) 2194, doi:10.1140/epjc/s10052-012-2194-8, arXiv:1208.3710.
- [34] CMS Collaboration, “Search for physics beyond the standard model in dilepton mass spectra in proton-proton collisions at $\sqrt{s} = 8$ TeV”, *JHEP* **04** (2015) 025, doi:10.1007/JHEP04(2015)025, arXiv:1412.6302.
- [35] R. Gavin, Y. Li, F. Petriello, and S. Quackenbush, “FEWZ 2.0: A code for hadronic Z production at next-to-next-to-leading order”, *Comput. Phys. Commun.* **182** (2011) 2388, doi:10.1016/j.cpc.2011.06.008, arXiv:1011.3540.
- [36] Y. Li and F. Petriello, “Combining QCD and electroweak corrections to dilepton production in the framework of the FEWZ simulation code”, *Phys. Rev. D* **86** (2012) 094034, doi:10.1103/PhysRevD.86.094034, arXiv:1208.5967.
- [37] A. V. Manohar, P. Nason, G. P. Salam, and G. Zanderighi, “The photon content of the proton”, *JHEP* **12** (2017) 046, doi:10.1007/JHEP12(2017)046, arXiv:1708.01256.
- [38] D. Bourilkov, “Photon-induced background for dilepton searches and measurements in pp collisions at 13 TeV”, (2016). arXiv:1606.00523.
- [39] D. Bourilkov, “Exploring the LHC landscape with dileptons”, (2016). arXiv:1609.08994.
- [40] G. D’Agostini, “A multidimensional unfolding method based on Bayes’ theorem”, *Nucl. Instrum. Meth. A* **362** (1995) 487, doi:10.1016/0168-9002(95)00274-X.
- [41] CMS Collaboration, “Measurement of the inclusive W and Z production cross sections in pp collisions at $\sqrt{s} = 7$ TeV with the CMS experiment”, *JHEP* **10** (2011) 132, doi:10.1007/JHEP10(2011)132, arXiv:1107.4789.
- [42] P. Golonka and Z. Was, “PHOTOS Monte Carlo: a precision tool for QED corrections in Z and W decays”, *Eur. Phys. J. C* **45** (2006) 97, doi:10.1140/epjc/s2005-02396-4, arXiv:hep-ph/0506026.
- [43] CMS Collaboration, “CMS luminosity measurement for the 2015 data taking period”, CMS Physics Analysis Summary CMS-PAS-LUM-15-001, 2015.
- [44] CMS Collaboration, “Measurements of differential production cross sections for a Z boson in association with jets in pp collisions at $\sqrt{s} = 8$ TeV”, *JHEP* **04** (2017) 022, doi:10.1007/JHEP04(2017)022, arXiv:1611.03844.

-
- [45] G. D. Lafferty and T. R. Wyatt, "Where to stick your data points: The treatment of measurements within wide bins", *Nucl. Instrum. Meth. A* **355** (1995) 541, doi:10.1016/0168-9002(94)01112-5.

A The CMS Collaboration

Yerevan Physics Institute, Yerevan, Armenia

A.M. Sirunyan, A. Tumasyan

Institut für Hochenergiephysik, Wien, Austria

W. Adam, F. Ambrogio, E. Asilar, T. Bergauer, J. Brandstetter, E. Brondolin, M. Dragicevic, J. Erö, A. Escalante Del Valle, M. Flechl, R. Frühwirth¹, V.M. Ghete, J. Hrubec, M. Jeitler¹, N. Krammer, I. Krätschmer, D. Liko, T. Madlener, I. Mikulec, N. Rad, H. Rohringer, J. Schieck¹, R. Schöfbeck, M. Spanring, D. Spitzbart, A. Taurok, W. Waltenberger, J. Wittmann, C.-E. Wulz¹, M. Zarucki

Institute for Nuclear Problems, Minsk, Belarus

V. Chekhovsky, V. Mossolov, J. Suarez Gonzalez

Universiteit Antwerpen, Antwerpen, Belgium

E.A. De Wolf, D. Di Croce, X. Janssen, J. Lauwers, M. Pieters, M. Van De Klundert, H. Van Haevermaet, P. Van Mechelen, N. Van Remortel

Vrije Universiteit Brussel, Brussel, Belgium

S. Abu Zeid, F. Blekman, J. D'Hondt, I. De Bruyn, J. De Clercq, K. Deroover, G. Flouris, D. Lontkovskyi, S. Lowette, I. Marchesini, S. Moortgat, L. Moreels, Q. Python, K. Skovpen, S. Tavernier, W. Van Doninck, P. Van Mulders, I. Van Parijs

Université Libre de Bruxelles, Bruxelles, Belgium

D. Beghin, B. Bilin, H. Brun, B. Clerboux, G. De Lentdecker, H. Delannoy, B. Dorney, G. Fasanella, L. Favart, R. Goldouzian, A. Grebenyuk, A.K. Kalsi, T. Lenzi, J. Luetic, N. Postiau, E. Starling, L. Thomas, C. Vander Velde, P. Vanlaer, D. Vannerom, Q. Wang

Ghent University, Ghent, Belgium

T. Cornelis, D. Dobur, A. Fagot, M. Gul, I. Khvastunov², D. Poyraz, C. Roskas, D. Trocino, M. Tytgat, W. Verbeke, B. Vermassen, M. Vit, N. Zaganidis

Université Catholique de Louvain, Louvain-la-Neuve, Belgium

H. Bakhshiansohi, O. Bondu, S. Brochet, G. Bruno, C. Caputo, P. David, C. Delaere, M. Delcourt, B. Francois, A. Giammanco, G. Krintiras, V. Lemaitre, A. Magitteri, A. Mertens, M. Musich, K. Piotrkowski, A. Saggio, M. Vidal Marono, S. Wertz, J. Zobec

Centro Brasileiro de Pesquisas Físicas, Rio de Janeiro, Brazil

F.L. Alves, G.A. Alves, L. Brito, G. Correia Silva, C. Hensel, A. Moraes, M.E. Pol, P. Rebello Teles

Universidade do Estado do Rio de Janeiro, Rio de Janeiro, Brazil

E. Belchior Batista Das Chagas, W. Carvalho, J. Chinellato³, E. Coelho, E.M. Da Costa, G.G. Da Silveira⁴, D. De Jesus Damiao, C. De Oliveira Martins, S. Fonseca De Souza, H. Malbouisson, D. Matos Figueiredo, M. Melo De Almeida, C. Mora Herrera, L. Mundim, H. Nogima, W.L. Prado Da Silva, L.J. Sanchez Rosas, A. Santoro, A. Sznajder, M. Thiel, E.J. Tonelli Manganote³, F. Torres Da Silva De Araujo, A. Vilela Pereira

Universidade Estadual Paulista ^a, Universidade Federal do ABC ^b, São Paulo, Brazil

S. Ahuja^a, C.A. Bernardes^a, L. Calligaris^a, T.R. Fernandez Perez Tomei^a, E.M. Gregores^b, P.G. Mercadante^b, S.F. Novaes^a, SandraS. Padula^a, D. Romero Abad^b

Institute for Nuclear Research and Nuclear Energy, Bulgarian Academy of Sciences, Sofia, Bulgaria

A. Aleksandrov, R. Hadjiiska, P. Iaydjiev, A. Marinov, M. Misheva, M. Rodozov, M. Shopova, G. Sultanov

University of Sofia, Sofia, Bulgaria

A. Dimitrov, L. Litov, B. Pavlov, P. Petkov

Beihang University, Beijing, China

W. Fang⁵, X. Gao⁵, L. Yuan

Institute of High Energy Physics, Beijing, China

M. Ahmad, J.G. Bian, G.M. Chen, H.S. Chen, M. Chen, Y. Chen, C.H. Jiang, D. Leggat, H. Liao, Z. Liu, F. Romeo, S.M. Shaheen, A. Spiezia, J. Tao, C. Wang, Z. Wang, E. Yazgan, H. Zhang, J. Zhao

State Key Laboratory of Nuclear Physics and Technology, Peking University, Beijing, China

Y. Ban, G. Chen, A. Levin, J. Li, L. Li, Q. Li, Y. Mao, S.J. Qian, D. Wang, Z. Xu

Tsinghua University, Beijing, China

Y. Wang

Universidad de Los Andes, Bogota, Colombia

C. Avila, A. Cabrera, C.A. Carrillo Montoya, L.F. Chaparro Sierra, C. Florez, C.F. González Hernández, M.A. Segura Delgado

University of Split, Faculty of Electrical Engineering, Mechanical Engineering and Naval Architecture, Split, Croatia

B. Courbon, N. Godinovic, D. Lelas, I. Puljak, T. Sculac

University of Split, Faculty of Science, Split, Croatia

Z. Antunovic, M. Kovac

Institute Rudjer Boskovic, Zagreb, Croatia

V. Brigljevic, D. Ferencek, K. Kadija, B. Mesic, A. Starodumov⁶, T. Susa

University of Cyprus, Nicosia, Cyprus

M.W. Ather, A. Attikis, G. Mavromanolakis, J. Mousa, C. Nicolaou, F. Ptochos, P.A. Razis, H. Rykaczewski

Charles University, Prague, Czech Republic

M. Finger⁷, M. Finger Jr.⁷

Escuela Politecnica Nacional, Quito, Ecuador

E. Ayala

Universidad San Francisco de Quito, Quito, Ecuador

E. Carrera Jarrin

Academy of Scientific Research and Technology of the Arab Republic of Egypt, Egyptian Network of High Energy Physics, Cairo, Egypt

A. Ellithi Kamel⁸, M.A. Mahmoud^{9,10}, E. Salama^{10,11}

National Institute of Chemical Physics and Biophysics, Tallinn, Estonia

S. Bhowmik, A. Carvalho Antunes De Oliveira, R.K. Dewanjee, K. Ehataht, M. Kadastik, M. Raidal, C. Veelken

Department of Physics, University of Helsinki, Helsinki, Finland

P. Eerola, H. Kirschenmann, J. Pekkanen, M. Voutilainen

Helsinki Institute of Physics, Helsinki, Finland

J. Havukainen, J.K. Heikkilä, T. Järvinen, V. Karimäki, R. Kinnunen, T. Lampén, K. Lassila-Perini, S. Laurila, S. Lehti, T. Lindén, P. Luukka, T. Mäenpää, H. Siikonen, E. Tuominen, J. Tuominiemi

Lappeenranta University of Technology, Lappeenranta, Finland

T. Tuuva

IRFU, CEA, Université Paris-Saclay, Gif-sur-Yvette, France

M. Besancon, F. Couderc, M. Dejardin, D. Denegri, J.L. Faure, F. Ferri, S. Ganjour, A. Givernaud, P. Gras, G. Hamel de Monchenault, P. Jarry, C. Leloup, E. Locci, J. Malcles, G. Negro, J. Rander, A. Rosowsky, M.Ö. Sahin, M. Titov

Laboratoire Leprince-Ringuet, Ecole polytechnique, CNRS/IN2P3, Université Paris-Saclay, Palaiseau, France

A. Abdulsalam¹², C. Amendola, I. Antropov, F. Beaudette, P. Busson, C. Charlot, R. Granier de Cassagnac, I. Kucher, S. Lisniak, A. Lobanov, J. Martin Blanco, M. Nguyen, C. Ochando, G. Ortona, P. Paganini, P. Pigard, R. Salerno, J.B. Sauvan, Y. Sirois, A.G. Stahl Leiton, A. Zabi, A. Zghiche

Université de Strasbourg, CNRS, IPHC UMR 7178, Strasbourg, France

J.-L. Agram¹³, J. Andrea, D. Bloch, J.-M. Brom, E.C. Chabert, V. Cherepanov, C. Collard, E. Conte¹³, J.-C. Fontaine¹³, D. Gelé, U. Goerlach, M. Jansová, A.-C. Le Bihan, N. Tonon, P. Van Hove

Centre de Calcul de l'Institut National de Physique Nucleaire et de Physique des Particules, CNRS/IN2P3, Villeurbanne, France

S. Gadrat

Université de Lyon, Université Claude Bernard Lyon 1, CNRS-IN2P3, Institut de Physique Nucléaire de Lyon, Villeurbanne, France

S. Beauceron, C. Bernet, G. Boudoul, N. Chanon, R. Chierici, D. Contardo, P. Depasse, H. El Mamouni, J. Fay, L. Finco, S. Gascon, M. Gouzevitch, G. Grenier, B. Ille, F. Lagarde, I.B. Laktineh, H. Lattaud, M. Lethuillier, L. Mirabito, A.L. Pequegnot, S. Perries, A. Popov¹⁴, V. Sordini, M. Vander Donckt, S. Viret, S. Zhang

Georgian Technical University, Tbilisi, Georgia

T. Toriashvili¹⁵

Tbilisi State University, Tbilisi, Georgia

Z. Tsamalaidze⁷

RWTH Aachen University, I. Physikalisches Institut, Aachen, Germany

C. Autermann, L. Feld, M.K. Kiesel, K. Klein, M. Lipinski, M. Preuten, M.P. Rauch, C. Schomakers, J. Schulz, M. Teroerde, B. Wittmer, V. Zhukov¹⁴

RWTH Aachen University, III. Physikalisches Institut A, Aachen, Germany

A. Albert, D. Duchardt, M. Endres, M. Erdmann, T. Esch, R. Fischer, S. Ghosh, A. Güth, T. Hebbeker, C. Heidemann, K. Hoepfner, H. Keller, S. Knutzen, L. Mastrolorenzo, M. Merschmeyer, A. Meyer, P. Millet, S. Mukherjee, T. Pook, M. Radziej, H. Reithler, M. Rieger, F. Scheuch, A. Schmidt, D. Teyssier

RWTH Aachen University, III. Physikalisches Institut B, Aachen, Germany

G. Flügge, O. Hlushchenko, B. Kargoll, T. Kress, A. Künsken, T. Müller, A. Nehr Korn, A. Nowack, C. Pistone, O. Pooth, H. Sert, A. Stahl¹⁶

Deutsches Elektronen-Synchrotron, Hamburg, Germany

M. Aldaya Martin, T. Arndt, C. Asawatangtrakuldee, I. Babounikau, K. Beernaert, O. Behnke, U. Behrens, A. Bermúdez Martínez, D. Bertsche, A.A. Bin Anuar, K. Borras¹⁷, V. Botta, A. Campbell, P. Connor, C. Contreras-Campana, F. Costanza, V. Danilov, A. De Wit, M.M. Defranchis, C. Diez Pardos, D. Domínguez Damiani, G. Eckerlin, T. Eichhorn, A. Elwood, E. Eren, E. Gallo¹⁸, A. Geiser, J.M. Grados Luyando, A. Grohsjean, P. Gunnellini, M. Guthoff, M. Haranko, A. Harb, J. Hauk, H. Jung, M. Kasemann, J. Keaveney, C. Kleinwort, J. Knolle, D. Krücker, W. Lange, A. Lelek, T. Lenz, K. Lipka, W. Lohmann¹⁹, R. Mankel, I.-A. Melzer-Pellmann, A.B. Meyer, M. Meyer, M. Missiroli, G. Mittag, J. Mnich, V. Myronenko, S.K. Pflitsch, D. Pitzl, A. Raspereza, M. Savitskyi, P. Saxena, P. Schütze, C. Schwanenberger, R. Shevchenko, A. Singh, N. Stefaniuk, H. Tholen, A. Vagnerini, G.P. Van Onsem, R. Walsh, Y. Wen, K. Wichmann, C. Wissing, O. Zenaiev

University of Hamburg, Hamburg, Germany

R. Aggleton, S. Bein, L. Benato, A. Benecke, V. Blobel, M. Centis Vignali, T. Dreyer, E. Garutti, D. Gonzalez, J. Haller, A. Hinzmann, A. Karavdina, G. Kasieczka, R. Klanner, R. Kogler, N. Kovalchuk, S. Kurz, V. Kutzner, J. Lange, D. Marconi, J. Multhaupt, M. Niedziela, D. Nowatschin, A. Perieanu, A. Reimers, O. Rieger, C. Scharf, P. Schleper, S. Schumann, J. Schwandt, J. Sonneveld, H. Stadie, G. Steinbrück, F.M. Stober, M. Stöver, D. Troendle, A. Vanhoefer, B. Vormwald

Karlsruher Institut fuer Technologie, Karlsruhe, Germany

M. Akbiyik, C. Barth, M. Baselga, S. Baur, E. Butz, R. Caspart, T. Chwalek, F. Colombo, W. De Boer, A. Dierlamm, N. Faltermann, B. Freund, M. Giffels, M.A. Harrendorf, F. Hartmann¹⁶, S.M. Heindl, U. Husemann, F. Kassel¹⁶, I. Katkov¹⁴, S. Kudella, H. Mildner, S. Mitra, M.U. Mozer, Th. Müller, M. Plagge, G. Quast, K. Rabbertz, M. Schröder, I. Shvetsov, G. Sieber, H.J. Simonis, R. Ulrich, S. Wayand, M. Weber, T. Weiler, S. Williamson, C. Wöhrmann, R. Wolf

Institute of Nuclear and Particle Physics (INPP), NCSR Demokritos, Aghia Paraskevi, Greece

G. Anagnostou, G. Daskalakis, T. Gerasis, A. Kyriakis, D. Loukas, G. Paspalaki, I. Topsis-Giotis

National and Kapodistrian University of Athens, Athens, Greece

G. Karathanasis, S. Kesisoglou, P. Kontaxakis, A. Panagiotou, N. Saoulidou, E. Tziaferi, K. Vellidis

National Technical University of Athens, Athens, Greece

K. Kousouris, I. Papakrivopoulos, G. Tsipolitis

University of Ioánnina, Ioánnina, Greece

I. Evangelou, C. Foudas, P. Giannelis, P. Katsoulis, P. Kokkas, S. Mallios, N. Manthos, I. Papadopoulos, E. Paradas, J. Strologas, F.A. Triantis, D. Tsitsonis

MTA-ELTE Lendület CMS Particle and Nuclear Physics Group, Eötvös Loránd University, Budapest, Hungary

M. Csanad, N. Filipovic, P. Major, M.I. Nagy, G. Pasztor, O. Surányi, G.I. Veres

Wigner Research Centre for Physics, Budapest, Hungary

G. Bencze, C. Hajdu, D. Horvath²⁰, Á. Hunyadi, F. Sikler, T.Á. Vámi, V. Veszpremi, G. Vesztergombi[†]

Institute of Nuclear Research ATOMKI, Debrecen, Hungary

N. Beni, S. Czellar, J. Karancsi²², A. Makovec, J. Molnar, Z. Szillasi

Institute of Physics, University of Debrecen, Debrecen, Hungary

M. Bartók²¹, P. Raics, Z.L. Trocsanyi, B. Ujvari

Indian Institute of Science (IISc), Bangalore, India

S. Choudhury, J.R. Komaragiri, P.C. Tiwari

National Institute of Science Education and Research, HBNI, Bhubaneswar, India

S. Bahinipati²³, C. Kar, P. Mal, K. Mandal, A. Nayak²⁴, D.K. Sahoo²³, S.K. Swain

Panjab University, Chandigarh, India

S. Bansal, S.B. Beri, V. Bhatnagar, S. Chauhan, R. Chawla, N. Dhingra, R. Gupta, A. Kaur, A. Kaur, M. Kaur, S. Kaur, R. Kumar, P. Kumari, M. Lohan, A. Mehta, K. Sandeep, S. Sharma, J.B. Singh, G. Walia

University of Delhi, Delhi, India

A. Bhardwaj, B.C. Choudhary, R.B. Garg, M. Gola, S. Keshri, Ashok Kumar, S. Malhotra, M. Naimuddin, P. Priyanka, K. Ranjan, Aashaq Shah, R. Sharma

Saha Institute of Nuclear Physics, HBNI, Kolkata, India

R. Bhardwaj²⁵, M. Bharti, R. Bhattacharya, S. Bhattacharya, U. Bhawandeep²⁵, D. Bhowmik, S. Dey, S. Dutt²⁵, S. Dutta, S. Ghosh, K. Mondal, S. Nandan, A. Purohit, P.K. Rout, A. Roy, S. Roy Chowdhury, S. Sarkar, M. Sharan, B. Singh, S. Thakur²⁵

Indian Institute of Technology Madras, Madras, India

P.K. Behera

Bhabha Atomic Research Centre, Mumbai, India

R. Chudasama, D. Dutta, V. Jha, V. Kumar, P.K. Netrakanti, L.M. Pant, P. Shukla

Tata Institute of Fundamental Research-A, Mumbai, India

T. Aziz, M.A. Bhat, S. Dugad, G.B. Mohanty, N. Sur, B. Sutar, RavindraKumar Verma

Tata Institute of Fundamental Research-B, Mumbai, India

S. Banerjee, S. Bhattacharya, S. Chatterjee, P. Das, M. Guchait, Sa. Jain, S. Kumar, M. Maity²⁶, G. Majumder, K. Mazumdar, N. Sahoo, T. Sarkar²⁶

Indian Institute of Science Education and Research (IISER), Pune, India

S. Chauhan, S. Dube, V. Hegde, A. Kapoor, K. Kothekar, S. Pandey, A. Rane, S. Sharma

Institute for Research in Fundamental Sciences (IPM), Tehran, Iran

S. Chenarani²⁷, E. Eskandari Tadavani, S.M. Etesami²⁷, M. Khakzad, M. Mohammadi Najafabadi, M. Naseri, F. Rezaei Hosseinabadi, B. Safarzadeh²⁸, M. Zeinali

University College Dublin, Dublin, Ireland

M. Felcini, M. Grunewald

INFN Sezione di Bari ^a, Università di Bari ^b, Politecnico di Bari ^c, Bari, Italy

M. Abbrescia^{a,b}, C. Calabria^{a,b}, A. Colaleo^a, D. Creanza^{a,c}, L. Cristella^{a,b}, N. De Filippis^{a,c}, M. De Palma^{a,b}, A. Di Florio^{a,b}, F. Errico^{a,b}, L. Fiore^a, A. Gelmi^{a,b}, G. Iaselli^{a,c}, S. Lezki^{a,b}, G. Maggi^{a,c}, M. Maggi^a, G. Miniello^{a,b}, S. My^{a,b}, S. Nuzzo^{a,b}, A. Pompili^{a,b}, G. Pugliese^{a,c}, R. Radogna^a, A. Ranieri^a, G. Selvaggi^{a,b}, A. Sharma^a, L. Silvestris^{a,16}, R. Venditti^a, P. Verwilligen^a, G. Zito^a

INFN Sezione di Bologna ^a, Università di Bologna ^b, Bologna, Italy

G. Abbiendi^a, C. Battilana^{a,b}, D. Bonacorsi^{a,b}, L. Borgonovi^{a,b}, S. Braibant-Giacomelli^{a,b}, L. Brigliadori^{a,b}, R. Campanini^{a,b}, P. Capiluppi^{a,b}, A. Castro^{a,b}, F.R. Cavallo^a, S.S. Chhibra^{a,b},

C. Ciocca^a, G. Codispoti^{a,b}, M. Cuffiani^{a,b}, G.M. Dallavalle^a, F. Fabbri^a, A. Fanfani^{a,b}, P. Giacomelli^a, C. Grandi^a, L. Guiducci^{a,b}, S. Marcellini^a, G. Masetti^a, A. Montanari^a, F.L. Navarria^{a,b}, A. Perrotta^a, A.M. Rossi^{a,b}, T. Rovelli^{a,b}, G.P. Siroli^{a,b}, N. Tosi^a

INFN Sezione di Catania ^a, Università di Catania ^b, Catania, Italy

S. Albergo^{a,b}, A. Di Mattia^a, R. Potenza^{a,b}, A. Tricomi^{a,b}, C. Tuve^{a,b}

INFN Sezione di Firenze ^a, Università di Firenze ^b, Firenze, Italy

G. Barbagli^a, K. Chatterjee^{a,b}, V. Ciulli^{a,b}, C. Civinini^a, R. D'Alessandro^{a,b}, E. Focardi^{a,b}, G. Latino, P. Lenzi^{a,b}, M. Meschini^a, S. Paoletti^a, L. Russo^{a,29}, G. Sguazzoni^a, D. Strom^a, L. Viliani^a

INFN Laboratori Nazionali di Frascati, Frascati, Italy

L. Benussi, S. Bianco, F. Fabbri, D. Piccolo, F. Primavera¹⁶

INFN Sezione di Genova ^a, Università di Genova ^b, Genova, Italy

F. Ferro^a, F. Ravera^{a,b}, E. Robutti^a, S. Tosi^{a,b}

INFN Sezione di Milano-Bicocca ^a, Università di Milano-Bicocca ^b, Milano, Italy

A. Benaglia^a, A. Beschi^b, L. Brianza^{a,b}, F. Brivio^{a,b}, V. Ciriolo^{a,b,16}, S. Di Guida^{a,d,16}, M.E. Dinardo^{a,b}, S. Fiorendi^{a,b}, S. Gennai^a, A. Ghezzi^{a,b}, P. Govoni^{a,b}, M. Malberti^{a,b}, S. Malvezzi^a, A. Massironi^{a,b}, D. Menasce^a, L. Moroni^a, M. Paganoni^{a,b}, D. Pedrini^a, S. Ragazzi^{a,b}, T. Tabarelli de Fatis^{a,b}

INFN Sezione di Napoli ^a, Università di Napoli 'Federico II' ^b, Napoli, Italy, Università della Basilicata ^c, Potenza, Italy, Università G. Marconi ^d, Roma, Italy

S. Buontempo^a, N. Cavallo^{a,c}, A. Di Crescenzo^{a,b}, F. Fabozzi^{a,c}, F. Fienga^a, G. Galati^a, A.O.M. Iorio^{a,b}, W.A. Khan^a, L. Lista^a, S. Meola^{a,d,16}, P. Paolucci^{a,16}, C. Sciacca^{a,b}, E. Voevodina^{a,b}

INFN Sezione di Padova ^a, Università di Padova ^b, Padova, Italy, Università di Trento ^c, Trento, Italy

P. Azzi^a, N. Bacchetta^a, D. Bisello^{a,b}, A. Boletti^{a,b}, A. Bragagnolo, R. Carlin^{a,b}, P. Checchia^a, P. De Castro Manzano^a, T. Dorigo^a, U. Dosselli^a, F. Gasparini^{a,b}, U. Gasparini^{a,b}, A. Gozzelino^a, S. Lacaprara^a, P. Lujan, M. Margoni^{a,b}, A.T. Meneguzzo^{a,b}, N. Pozzobon^{a,b}, P. Ronchese^{a,b}, R. Rossin^{a,b}, A. Tiko, E. Torassa^a, S. Ventura^a, M. Zanetti^{a,b}, P. Zotto^{a,b}, G. Zumerle^{a,b}

INFN Sezione di Pavia ^a, Università di Pavia ^b, Pavia, Italy

A. Braghieri^a, A. Magnani^a, P. Montagna^{a,b}, S.P. Ratti^{a,b}, V. Re^a, M. Ressegotti^{a,b}, C. Riccardi^{a,b}, P. Salvini^a, I. Vai^{a,b}, P. Vitulo^{a,b}

INFN Sezione di Perugia ^a, Università di Perugia ^b, Perugia, Italy

L. Alunni Solestizi^{a,b}, M. Biasini^{a,b}, G.M. Bilei^a, C. Cecchi^{a,b}, D. Ciangottini^{a,b}, L. Fanò^{a,b}, P. Lariccia^{a,b}, E. Manoni^a, G. Mantovani^{a,b}, V. Mariani^{a,b}, M. Menichelli^a, A. Rossi^{a,b}, A. Santocchia^{a,b}, D. Spiga^a

INFN Sezione di Pisa ^a, Università di Pisa ^b, Scuola Normale Superiore di Pisa ^c, Pisa, Italy

K. Androsov^a, P. Azzurri^a, G. Bagliesi^a, L. Bianchini^a, T. Boccali^a, L. Borrello, R. Castaldi^a, M.A. Ciocci^{a,b}, R. Dell'Orso^a, G. Fedi^a, L. Giannini^{a,c}, A. Giassi^a, M.T. Grippo^a, F. Ligabue^{a,c}, E. Manca^{a,c}, G. Mandorli^{a,c}, A. Messineo^{a,b}, F. Palla^a, A. Rizzi^{a,b}, P. Spagnolo^a, R. Tenchini^a, G. Tonelli^{a,b}, A. Venturi^a, P.G. Verdini^a

INFN Sezione di Roma ^a, Sapienza Università di Roma ^b, Rome, Italy

L. Barone^{a,b}, F. Cavallari^a, M. Cipriani^{a,b}, N. Daci^a, D. Del Re^{a,b}, E. Di Marco^{a,b}, M. Diemoz^a,

S. Gelli^{a,b}, E. Longo^{a,b}, B. Marzocchi^{a,b}, P. Meridiani^a, G. Organtini^{a,b}, F. Pandolfi^a, R. Paramatti^{a,b}, F. Preiato^{a,b}, S. Rahatlou^{a,b}, C. Rovelli^a, F. Santanastasio^{a,b}

INFN Sezione di Torino ^a, Università di Torino ^b, Torino, Italy, Università del Piemonte Orientale ^c, Novara, Italy

N. Amapane^{a,b}, R. Arcidiacono^{a,c}, S. Argiro^{a,b}, M. Arneodo^{a,c}, N. Bartosik^a, R. Bellan^{a,b}, C. Biino^a, N. Cartiglia^a, F. Cenna^{a,b}, S. Cometti, M. Costa^{a,b}, R. Covarelli^{a,b}, N. Demaria^a, B. Kiani^{a,b}, C. Mariotti^a, S. Maselli^a, E. Migliore^{a,b}, V. Monaco^{a,b}, E. Monteil^{a,b}, M. Monteno^a, M.M. Obertino^{a,b}, L. Pacher^{a,b}, N. Pastrone^a, M. Pelliccioni^a, G.L. Pinna Angioni^{a,b}, A. Romero^{a,b}, M. Ruspa^{a,c}, R. Sacchi^{a,b}, K. Shchelina^{a,b}, V. Sola^a, A. Solano^{a,b}, D. Soldi, A. Staiano^a

INFN Sezione di Trieste ^a, Università di Trieste ^b, Trieste, Italy

S. Belforte^a, V. Candelise^{a,b}, M. Casarsa^a, F. Cossutti^a, G. Della Ricca^{a,b}, F. Vazzoler^{a,b}, A. Zanetti^a

Kyungpook National University, Daegu, Korea

D.H. Kim, G.N. Kim, M.S. Kim, J. Lee, S. Lee, S.W. Lee, C.S. Moon, Y.D. Oh, S. Sekmen, D.C. Son, Y.C. Yang

Chonnam National University, Institute for Universe and Elementary Particles, Kwangju, Korea

H. Kim, D.H. Moon, G. Oh

Hanyang University, Seoul, Korea

J. Goh, T.J. Kim

Korea University, Seoul, Korea

S. Cho, S. Choi, Y. Go, D. Gyun, S. Ha, B. Hong, Y. Jo, K. Lee, K.S. Lee, S. Lee, J. Lim, S.K. Park, Y. Roh

Sejong University, Seoul, Korea

H.S. Kim

Seoul National University, Seoul, Korea

J. Almond, J. Kim, J.S. Kim, H. Lee, K. Lee, K. Nam, S.B. Oh, D. Pai, B.C. Radburn-Smith, S.h. Seo, U.K. Yang, H.D. Yoo, G.B. Yu

University of Seoul, Seoul, Korea

D. Jeon, H. Kim, J.H. Kim, J.S.H. Lee, I.C. Park

Sungkyunkwan University, Suwon, Korea

Y. Choi, C. Hwang, J. Lee, I. Yu

Vilnius University, Vilnius, Lithuania

V. Dudenias, A. Juodagalvis, J. Vaitkus

National Centre for Particle Physics, Universiti Malaya, Kuala Lumpur, Malaysia

I. Ahmed, Z.A. Ibrahim, M.A.B. Md Ali³⁰, F. Mohamad Idris³¹, W.A.T. Wan Abdullah, M.N. Yusli, Z. Zolkapli

Centro de Investigacion y de Estudios Avanzados del IPN, Mexico City, Mexico

H. Castilla-Valdez, E. De La Cruz-Burelo, M.C. Duran-Osuna, I. Heredia-De La Cruz³², R. Lopez-Fernandez, J. Mejia Guisao, R.I. Rabadan-Trejo, G. Ramirez-Sanchez, R Reyes-Almanza, A. Sanchez-Hernandez

Universidad Iberoamericana, Mexico City, Mexico

S. Carrillo Moreno, C. Oropeza Barrera, F. Vazquez Valencia

Benemerita Universidad Autonoma de Puebla, Puebla, Mexico

J. Eysermans, I. Pedraza, H.A. Salazar Ibarquen, C. Uribe Estrada

Universidad Autónoma de San Luis Potosí, San Luis Potosí, Mexico

A. Morelos Pineda

University of Auckland, Auckland, New Zealand

D. Krofcheck

University of Canterbury, Christchurch, New Zealand

S. Bheesette, P.H. Butler

National Centre for Physics, Quaid-I-Azam University, Islamabad, Pakistan

A. Ahmad, M. Ahmad, M.I. Asghar, Q. Hassan, H.R. Hoorani, A. Saddique, M.A. Shah, M. Shoaib, M. Waqas

National Centre for Nuclear Research, Swierk, Poland

H. Bialkowska, M. Bluj, B. Boimska, T. Frueboes, M. Górski, M. Kazana, K. Nawrocki, M. Szleper, P. Traczyk, P. Zalewski

Institute of Experimental Physics, Faculty of Physics, University of Warsaw, Warsaw, Poland

K. Bunkowski, A. Byszuk³³, K. Doroba, A. Kalinowski, M. Konecki, J. Krolikowski, M. Misiura, M. Olszewski, A. Pyskir, M. Walczak

Laboratório de Instrumentação e Física Experimental de Partículas, Lisboa, Portugal

P. Bargassa, C. Beirão Da Cruz E Silva, A. Di Francesco, P. Faccioli, B. Galinhas, M. Gallinaro, J. Hollar, N. Leonardo, L. Lloret Iglesias, M.V. Nemallapudi, J. Seixas, G. Strong, O. Toldaiev, D. Vadrucio, J. Varela

Joint Institute for Nuclear Research, Dubna, Russia

M. Gavrilenko, A. Golunov, I. Golutvin, N. Gorbounov, I. Gorbunov, A. Kamenev, V. Karjavin, V. Korenkov, A. Lanev, A. Malakhov, V. Matveev^{34,35}, P. Moisenz, V. Palichik, V. Perelygin, M. Savina, S. Shmatov, V. Smirnov, N. Voytishin, A. Zarubin

Petersburg Nuclear Physics Institute, Gatchina (St. Petersburg), Russia

V. Golovtsov, Y. Ivanov, V. Kim³⁶, E. Kuznetsova³⁷, P. Levchenko, V. Murzin, V. Oreshkin, I. Smirnov, D. Sosnov, V. Sulimov, L. Uvarov, S. Vavilov, A. Vorobyev

Institute for Nuclear Research, Moscow, Russia

Yu. Andreev, A. Dermenev, S. Gninenko, N. Golubev, A. Karneyeu, M. Kirsanov, N. Krasnikov, A. Pashenkov, D. Tlisov, A. Toropin

Institute for Theoretical and Experimental Physics, Moscow, Russia

V. Epshteyn, V. Gavrilov, N. Lychkovskaya, V. Popov, I. Pozdnyakov, G. Safronov, A. Spiridonov, A. Steppenov, V. Stolin, M. Toms, E. Vlasov, A. Zhokin

Moscow Institute of Physics and Technology, Moscow, Russia

T. Aushev, A. Bylinkin³⁵

National Research Nuclear University 'Moscow Engineering Physics Institute' (MEPhI), Moscow, Russia

M. Chadeeva³⁸, P. Parygin, D. Philippov, S. Polikarpov³⁸, E. Popova, V. Rusinov

P.N. Lebedev Physical Institute, Moscow, Russia

V. Andreev, M. Azarkin³⁵, I. Dremin³⁵, M. Kirakosyan³⁵, S.V. Rusakov, A. Terkulov

Skobeltsyn Institute of Nuclear Physics, Lomonosov Moscow State University, Moscow, Russia

A. Baskakov, A. Belyaev, E. Boos, V. Bunichev, M. Dubinin³⁹, L. Dudko, A. Ershov, V. Klyukhin, O. Kodolova, I. Lokhtin, I. Miagkov, S. Obraztsov, M. Perfilov, V. Savrin, A. Snigirev

Novosibirsk State University (NSU), Novosibirsk, Russia

V. Blinov⁴⁰, T. Dimova⁴⁰, L. Kardapoltsev⁴⁰, D. Shtol⁴⁰, Y. Skovpen⁴⁰

Institute for High Energy Physics of National Research Centre 'Kurchatov Institute', Protvino, Russia

I. Azhgirey, I. Bayshev, S. Bitioukov, D. Elumakhov, A. Godizov, V. Kachanov, A. Kalinin, D. Konstantinov, P. Mandrik, V. Petrov, R. Ryutin, S. Slabospitskii, A. Sobol, S. Troshin, N. Tyurin, A. Uzunian, A. Volkov

National Research Tomsk Polytechnic University, Tomsk, Russia

A. Babaev, S. Baidali

University of Belgrade, Faculty of Physics and Vinca Institute of Nuclear Sciences, Belgrade, Serbia

P. Adzic⁴¹, P. Cirkovic, D. Devetak, M. Dordevic, J. Milosevic

Centro de Investigaciones Energéticas Medioambientales y Tecnológicas (CIEMAT), Madrid, Spain

J. Alcaraz Maestre, A. Álvarez Fernández, I. Bachiller, M. Barrio Luna, J.A. Brochero Cifuentes, M. Cerrada, N. Colino, B. De La Cruz, A. Delgado Peris, C. Fernandez Bedoya, J.P. Fernández Ramos, J. Flix, M.C. Fouz, O. Gonzalez Lopez, S. Goy Lopez, J.M. Hernandez, M.I. Josa, D. Moran, A. Pérez-Calero Yzquierdo, J. Puerta Pelayo, I. Redondo, L. Romero, M.S. Soares, A. Triossi

Universidad Autónoma de Madrid, Madrid, Spain

C. Albajar, J.F. de Trocóniz

Universidad de Oviedo, Oviedo, Spain

J. Cuevas, C. Erice, J. Fernandez Menendez, S. Folgueras, I. Gonzalez Caballero, J.R. González Fernández, E. Palencia Cortezon, V. Rodríguez Bouza, S. Sanchez Cruz, P. Vischia, J.M. Vizán García

Instituto de Física de Cantabria (IFCA), CSIC-Universidad de Cantabria, Santander, Spain

I.J. Cabrillo, A. Calderon, B. Chazin Quero, J. Duarte Campderros, M. Fernandez, P.J. Fernández Manteca, A. García Alonso, J. Garcia-Ferrero, G. Gomez, A. Lopez Virto, J. Marco, C. Martinez Rivero, P. Martinez Ruiz del Arbol, F. Matorras, J. Piedra Gomez, C. Prieels, T. Rodrigo, A. Ruiz-Jimeno, L. Scodellaro, N. Trevisani, I. Vila, R. Vilar Cortabitarte

CERN, European Organization for Nuclear Research, Geneva, Switzerland

D. Abbaneo, B. Akgun, E. Auffray, P. Baillon, A.H. Ball, D. Barney, J. Bendavid, M. Bianco, A. Bocci, C. Botta, T. Camporesi, M. Cepeda, G. Cerminara, E. Chapon, Y. Chen, G. Cucciati, D. d'Enterria, A. Dabrowski, V. Daponte, A. David, A. De Roeck, N. Deelen, M. Dobson, T. du Pree, M. Dünser, N. Dupont, A. Elliott-Peisert, P. Everaerts, F. Fallavollita⁴², D. Fasanella, G. Franzoni, J. Fulcher, W. Funk, D. Gigi, A. Gilbert, K. Gill, F. Glege, D. Gulhan, J. Hegeman, V. Innocente, A. Jafari, P. Janot, O. Karacheban¹⁹, J. Kieseler, A. Kornmayer, M. Krammer¹, C. Lange, P. Lecoq, C. Lourenço, L. Malgeri, M. Mannelli, F. Meijers, J.A. Merlin, S. Mersi,

E. Meschi, P. Milenovic⁴³, F. Moortgat, M. Mulders, J. Ngadiuba, S. Orfanelli, L. Orsini, F. Pantaleo¹⁶, L. Pape, E. Perez, M. Peruzzi, A. Petrilli, G. Petrucciani, A. Pfeiffer, M. Pierini, F.M. Pitters, D. Rabady, A. Racz, T. Reis, G. Rolandi⁴⁴, M. Rovere, H. Sakulin, C. Schäfer, C. Schwick, M. Seidel, M. Selvaggi, A. Sharma, P. Silva, P. Sphicas⁴⁵, A. Stakia, J. Steggemann, M. Tosi, D. Treille, A. Tsirou, V. Veckalns⁴⁶, W.D. Zeuner

Paul Scherrer Institut, Villigen, Switzerland

W. Bertl[†], L. Caminada⁴⁷, K. Deiters, W. Erdmann, R. Horisberger, Q. Ingram, H.C. Kaestli, D. Kotlinski, U. Langenegger, T. Rohe, S.A. Wiederkehr

ETH Zurich - Institute for Particle Physics and Astrophysics (IPA), Zurich, Switzerland

M. Backhaus, L. Bäni, P. Berger, N. Chernyavskaya, G. Dissertori, M. Dittmar, M. Donegà, C. Dorfer, C. Grab, C. Heidegger, D. Hits, J. Hoss, T. Klijnsma, W. Lustermann, R.A. Manzoni, M. Marionneau, M.T. Meinhard, F. Micheli, P. Musella, F. Nessi-Tedaldi, J. Pata, F. Pauss, G. Perrin, L. Perrozzi, S. Pigazzini, M. Quittnat, D. Ruini, D.A. Sanz Becerra, M. Schönenberger, L. Shchutska, V.R. Tavolaro, K. Theofilatos, M.L. Vesterbacka Olsson, R. Wallny, D.H. Zhu

Universität Zürich, Zurich, Switzerland

T.K. Aarrestad, C. Amsler⁴⁸, D. Brzhechko, M.F. Canelli, A. De Cosa, R. Del Burgo, S. Donato, C. Galloni, T. Hreus, B. Kilminster, I. Neutelings, D. Pinna, G. Rauco, P. Robmann, D. Salerno, K. Schweiger, C. Seitz, Y. Takahashi, A. Zucchetta

National Central University, Chung-Li, Taiwan

Y.H. Chang, K.y. Cheng, T.H. Doan, Sh. Jain, R. Khurana, C.M. Kuo, W. Lin, A. Pozdnyakov, S.S. Yu

National Taiwan University (NTU), Taipei, Taiwan

P. Chang, Y. Chao, K.F. Chen, P.H. Chen, W.-S. Hou, Arun Kumar, Y.y. Li, R.-S. Lu, E. Paganis, A. Psallidas, A. Steen, J.f. Tsai

Chulalongkorn University, Faculty of Science, Department of Physics, Bangkok, Thailand

B. Asavapibhop, N. Srimanobhas, N. Suwonjandee

Çukurova University, Physics Department, Science and Art Faculty, Adana, Turkey

M.N. Bakirci⁴⁹, A. Bat, F. Boran, S. Cerci⁵⁰, S. Damarseckin, Z.S. Demiroglu, F. Dolek, C. Dozen, E. Eskut, S. Girgis, G. Gokbulut, Y. Guler, E. Gurpinar, I. Hos⁵¹, C. Isik, E.E. Kangal⁵², O. Kara, U. Kiminsu, M. Oglakci, G. Onengut, K. Ozdemir⁵³, A. Polatoz, D. Sunar Cerci⁵⁰, U.G. Tok, H. Topakli⁴⁹, S. Turkcapar, I.S. Zorbakir, C. Zorbilmez

Middle East Technical University, Physics Department, Ankara, Turkey

B. Isildak⁵⁴, G. Karapinar⁵⁵, M. Yalvac, M. Zeyrek

Bogazici University, Istanbul, Turkey

I.O. Atakisi, E. Gülmez, M. Kaya⁵⁶, O. Kaya⁵⁷, S. Ozkorucuklu⁵⁸, S. Tekten, E.A. Yetkin⁵⁹

Istanbul Technical University, Istanbul, Turkey

M.N. Agaras, S. Atay, A. Cakir, K. Cankocak, Y. Komurcu, S. Sen⁶⁰

Institute for Scintillation Materials of National Academy of Science of Ukraine, Kharkov, Ukraine

B. Grynyov

National Scientific Center, Kharkov Institute of Physics and Technology, Kharkov, Ukraine

L. Levchuk

University of Bristol, Bristol, United Kingdom

F. Ball, L. Beck, J.J. Brooke, D. Burns, E. Clement, D. Cussans, O. Davignon, H. Flacher, J. Goldstein, G.P. Heath, H.F. Heath, L. Kreczko, D.M. Newbold⁶¹, S. Paramesvaran, B. Penning, T. Sakuma, D. Smith, V.J. Smith, J. Taylor, A. Titterton

Rutherford Appleton Laboratory, Didcot, United Kingdom

K.W. Bell, A. Belyaev⁶², C. Brew, R.M. Brown, D. Cieri, D.J.A. Cockerill, J.A. Coughlan, K. Harder, S. Harper, J. Linacre, E. Olaiya, D. Petyt, C.H. Shepherd-Themistocleous, A. Thea, I.R. Tomalin, T. Williams, W.J. Womersley

Imperial College, London, United Kingdom

G. Auzinger, R. Bainbridge, P. Bloch, J. Borg, S. Breeze, O. Buchmuller, A. Bundock, S. Casasso, D. Colling, L. Corpe, P. Dauncey, G. Davies, M. Della Negra, R. Di Maria, Y. Haddad, G. Hall, G. Iles, T. James, M. Komm, C. Laner, L. Lyons, A.-M. Magnan, S. Malik, A. Martelli, J. Nash⁶³, A. Nikitenko⁶, V. Palladino, M. Pesaresi, A. Richards, A. Rose, E. Scott, C. Seez, A. Shtipliyski, G. Singh, M. Stoye, T. Strebler, S. Summers, A. Tapper, K. Uchida, T. Virdee¹⁶, N. Wardle, D. Winterbottom, J. Wright, S.C. Zenz

Brunel University, Uxbridge, United Kingdom

J.E. Cole, P.R. Hobson, A. Khan, P. Kyberd, C.K. Mackay, A. Morton, I.D. Reid, L. Teodorescu, S. Zahid

Baylor University, Waco, USA

K. Call, J. Dittmann, K. Hatakeyama, H. Liu, C. Madrid, B. McMaster, N. Pastika, C. Smith

Catholic University of America, Washington, DC, USA

R. Bartek, A. Dominguez

The University of Alabama, Tuscaloosa, USA

A. Buccilli, S.I. Cooper, C. Henderson, P. Rumerio, C. West

Boston University, Boston, USA

D. Arcaro, T. Bose, D. Gastler, D. Rankin, C. Richardson, J. Rohlf, L. Sulak, D. Zou

Brown University, Providence, USA

G. Benelli, X. Coubez, D. Cutts, M. Hadley, J. Hakala, U. Heintz, J.M. Hogan⁶⁴, K.H.M. Kwok, E. Laird, G. Landsberg, J. Lee, Z. Mao, M. Narain, J. Pazzini, S. Piperov, S. Sagir⁶⁵, R. Syarif, E. Usai, D. Yu

University of California, Davis, Davis, USA

R. Band, C. Brainerd, R. Breedon, D. Burns, M. Calderon De La Barca Sanchez, M. Chertok, J. Conway, R. Conway, P.T. Cox, R. Erbacher, C. Flores, G. Funk, W. Ko, O. Kukral, R. Lander, C. Mclean, M. Mulhearn, D. Pellett, J. Pilot, S. Shalhout, M. Shi, D. Stolp, D. Taylor, K. Tos, M. Tripathi, Z. Wang, F. Zhang

University of California, Los Angeles, USA

M. Bachtis, C. Bravo, R. Cousins, A. Dasgupta, A. Florent, J. Hauser, M. Ignatenko, N. Mccoll, S. Regnard, D. Saltzberg, C. Schnaible, V. Valuev

University of California, Riverside, Riverside, USA

E. Bouvier, K. Burt, R. Clare, J.W. Gary, S.M.A. Ghiasi Shirazi, G. Hanson, G. Karapostoli, E. Kennedy, F. Lacroix, O.R. Long, M. Olmedo Negrete, M.I. Paneva, W. Si, L. Wang, H. Wei, S. Wimpenny, B.R. Yates

University of California, San Diego, La Jolla, USA

J.G. Branson, S. Cittolin, M. Derdzinski, R. Gerosa, D. Gilbert, B. Hashemi, A. Holzner, D. Klein, G. Kole, V. Krutelyov, J. Letts, M. Masciovecchio, D. Olivito, S. Padhi, M. Pieri, M. Sani, V. Sharma, S. Simon, M. Tadel, A. Vartak, S. Wasserbaech⁶⁶, J. Wood, F. Würthwein, A. Yagil, G. Zevi Della Porta

University of California, Santa Barbara - Department of Physics, Santa Barbara, USA

N. Amin, R. Bhandari, J. Bradmiller-Feld, C. Campagnari, M. Citron, A. Dishaw, V. Dutta, M. Franco Sevilla, L. Gouskos, R. Heller, J. Incandela, A. Ovcharova, H. Qu, J. Richman, D. Stuart, I. Suarez, S. Wang, J. Yoo

California Institute of Technology, Pasadena, USA

D. Anderson, A. Bornheim, J.M. Lawhorn, H.B. Newman, T.Q. Nguyen, M. Spiropulu, J.R. Vlimant, R. Wilkinson, S. Xie, Z. Zhang, R.Y. Zhu

Carnegie Mellon University, Pittsburgh, USA

M.B. Andrews, T. Ferguson, T. Mudholkar, M. Paulini, M. Sun, I. Vorobiev, M. Weinberg

University of Colorado Boulder, Boulder, USA

J.P. Cumalat, W.T. Ford, F. Jensen, A. Johnson, M. Krohn, S. Leontsinis, E. MacDonald, T. Mulholland, K. Stenson, K.A. Ulmer, S.R. Wagner

Cornell University, Ithaca, USA

J. Alexander, J. Chaves, Y. Cheng, J. Chu, A. Datta, K. McDermott, N. Mirman, J.R. Patterson, D. Quach, A. Rinkevicius, A. Ryd, L. Skinnari, L. Soffi, S.M. Tan, Z. Tao, J. Thom, J. Tucker, P. Wittich, M. Zientek

Fermi National Accelerator Laboratory, Batavia, USA

S. Abdullin, M. Albrow, M. Alyari, G. Apollinari, A. Apresyan, A. Apyan, S. Banerjee, L.A.T. Bauerdick, A. Beretvas, J. Berryhill, P.C. Bhat, G. Bolla[†], K. Burkett, J.N. Butler, A. Canepa, G.B. Cerati, H.W.K. Cheung, F. Chlebana, M. Cremonesi, J. Duarte, V.D. Elvira, J. Freeman, Z. Gecse, E. Gottschalk, L. Gray, D. Green, S. Grünendahl, O. Gutsche, J. Hanlon, R.M. Harris, S. Hasegawa, J. Hirschauer, Z. Hu, B. Jayatilaka, S. Jindariani, M. Johnson, U. Joshi, B. Klima, M.J. Kortelainen, B. Kreis, S. Lammel, D. Lincoln, R. Lipton, M. Liu, T. Liu, J. Lykken, K. Maeshima, J.M. Marraffino, D. Mason, P. McBride, P. Merkel, S. Mrenna, S. Nahn, V. O'Dell, K. Pedro, C. Pena, O. Prokofyev, G. Rakness, L. Ristori, A. Savoy-Navarro⁶⁷, B. Schneider, E. Sexton-Kennedy, A. Soha, W.J. Spalding, L. Spiegel, S. Stoynev, J. Strait, N. Strobbe, L. Taylor, S. Tkaczyk, N.V. Tran, L. Uplegger, E.W. Vaandering, C. Vernieri, M. Verzocchi, R. Vidal, M. Wang, H.A. Weber, A. Whitbeck

University of Florida, Gainesville, USA

D. Acosta, P. Avery, P. Bortignon, D. Bourilkov, A. Brinkerhoff, L. Cadamuro, A. Carnes, M. Carver, D. Curry, R.D. Field, S.V. Gleyzer, B.M. Joshi, J. Konigsberg, A. Korytov, P. Ma, K. Matchev, H. Mei, G. Mitselmakher, K. Shi, D. Sperka, J. Wang, S. Wang

Florida International University, Miami, USA

Y.R. Joshi, S. Linn

Florida State University, Tallahassee, USA

A. Ackert, T. Adams, A. Askew, S. Hagopian, V. Hagopian, K.F. Johnson, T. Kolberg, G. Martinez, T. Perry, H. Prosper, A. Saha, A. Santra, V. Sharma, R. Yohay

Florida Institute of Technology, Melbourne, USA

M.M. Baarmand, V. Bhopatkar, S. Colafranceschi, M. Hohlmann, D. Noonan, M. Rahmani, T. Roy, F. Yumiceva

University of Illinois at Chicago (UIC), Chicago, USA

M.R. Adams, L. Apanasevich, D. Berry, R.R. Betts, R. Cavanaugh, X. Chen, S. Dittmer, O. Evdokimov, C.E. Gerber, D.A. Hangal, D.J. Hofman, K. Jung, J. Kamin, C. Mills, I.D. Sandoval Gonzalez, M.B. Tonjes, N. Varelas, H. Wang, X. Wang, Z. Wu, J. Zhang

The University of Iowa, Iowa City, USA

M. Alhusseini, B. Bilki⁶⁸, W. Clarida, K. Dilsiz⁶⁹, S. Durgut, R.P. Gandrajula, M. Haytmyradov, V. Khristenko, J.-P. Merlo, A. Mestvirishvili, A. Moeller, J. Nachtman, H. Ogul⁷⁰, Y. Onel, F. Ozok⁷¹, A. Penzo, C. Snyder, E. Tiras, J. Wetzel

Johns Hopkins University, Baltimore, USA

B. Blumenfeld, A. Cocoros, N. Eminizer, D. Fehling, L. Feng, A.V. Gritsan, W.T. Hung, P. Maksimovic, J. Roskes, U. Sarica, M. Swartz, M. Xiao, C. You

The University of Kansas, Lawrence, USA

A. Al-bataineh, P. Baringer, A. Bean, S. Boren, J. Bowen, J. Castle, S. Khalil, A. Kropivnitskaya, D. Majumder, W. Mcbrayer, M. Murray, C. Rogan, S. Sanders, E. Schmitz, J.D. Tapia Takaki, Q. Wang

Kansas State University, Manhattan, USA

A. Ivanov, K. Kaadze, D. Kim, Y. Maravin, D.R. Mendis, T. Mitchell, A. Modak, A. Mohammadi, L.K. Saini, N. Skhirtladze

Lawrence Livermore National Laboratory, Livermore, USA

F. Rebassoo, D. Wright

University of Maryland, College Park, USA

A. Baden, O. Baron, A. Belloni, S.C. Eno, Y. Feng, C. Ferraioli, N.J. Hadley, S. Jabeen, G.Y. Jeng, R.G. Kellogg, J. Kunkle, A.C. Mignerey, F. Ricci-Tam, Y.H. Shin, A. Skuja, S.C. Tonwar, K. Wong

Massachusetts Institute of Technology, Cambridge, USA

D. Abercrombie, B. Allen, V. Azzolini, A. Baty, G. Bauer, R. Bi, S. Brandt, W. Busza, I.A. Cali, M. D'Alfonso, Z. Demiragli, G. Gomez Ceballos, M. Goncharov, P. Harris, D. Hsu, M. Hu, Y. Iiyama, G.M. Innocenti, M. Klute, D. Kovalskyi, Y.-J. Lee, P.D. Luckey, B. Maier, A.C. Marini, C. McGinn, C. Mironov, S. Narayanan, X. Niu, C. Paus, C. Roland, G. Roland, G.S.F. Stephans, K. Sumorok, K. Tatar, D. Velicanu, J. Wang, T.W. Wang, B. Wyslouch, S. Zhaozhong

University of Minnesota, Minneapolis, USA

A.C. Benvenuti, R.M. Chatterjee, A. Evans, P. Hansen, S. Kalafut, Y. Kubota, Z. Lesko, J. Mans, S. Nourbakhsh, N. Ruckstuhl, R. Rusack, J. Turkewitz, M.A. Wadud

University of Mississippi, Oxford, USA

J.G. Acosta, S. Oliveros

University of Nebraska-Lincoln, Lincoln, USA

E. Avdeeva, K. Bloom, D.R. Claes, C. Fangmeier, F. Golf, R. Gonzalez Suarez, R. Kamalieddin, I. Kravchenko, J. Monroy, J.E. Siado, G.R. Snow, B. Stieger

State University of New York at Buffalo, Buffalo, USA

A. Godshalk, C. Harrington, I. Iashvili, A. Kharchilava, D. Nguyen, A. Parker, S. Rappoccio, B. Roozbahani

Northeastern University, Boston, USA

G. Alverson, E. Barberis, C. Freer, A. Hortiangtham, D.M. Morse, T. Orimoto, R. Teixeira De Lima, T. Wamorkar, B. Wang, A. Wisecarver, D. Wood

Northwestern University, Evanston, USA

S. Bhattacharya, O. Charaf, K.A. Hahn, N. Mucia, N. Odell, M.H. Schmitt, K. Sung, M. Trovato, M. Velasco

University of Notre Dame, Notre Dame, USA

R. Bucci, N. Dev, M. Hildreth, K. Hurtado Anampa, C. Jessop, D.J. Karmgard, N. Kellams, K. Lannon, W. Li, N. Loukas, N. Marinelli, F. Meng, C. Mueller, Y. Musienko³⁴, M. Planer, A. Reinsvold, R. Ruchti, P. Siddireddy, G. Smith, S. Taroni, M. Wayne, A. Wightman, M. Wolf, A. Woodard

The Ohio State University, Columbus, USA

J. Alimena, L. Antonelli, B. Bylsma, L.S. Durkin, S. Flowers, B. Francis, A. Hart, C. Hill, W. Ji, T.Y. Ling, W. Luo, B.L. Winer, H.W. Wulsin

Princeton University, Princeton, USA

S. Cooperstein, P. Elmer, J. Hardenbrook, P. Hebda, S. Higginbotham, A. Kalogeropoulos, D. Lange, M.T. Lucchini, J. Luo, D. Marlow, K. Mei, I. Ojalvo, J. Olsen, C. Palmer, P. Piroué, J. Salfeld-Nebgen, D. Stickland, C. Tully

University of Puerto Rico, Mayaguez, USA

S. Malik, S. Norberg

Purdue University, West Lafayette, USA

A. Barker, V.E. Barnes, S. Das, L. Gutay, M. Jones, A.W. Jung, A. Khatiwada, B. Mahakud, D.H. Miller, N. Neumeister, C.C. Peng, H. Qiu, J.F. Schulte, J. Sun, F. Wang, R. Xiao, W. Xie

Purdue University Northwest, Hammond, USA

T. Cheng, J. Dolen, N. Parashar

Rice University, Houston, USA

Z. Chen, K.M. Ecklund, S. Freed, F.J.M. Geurts, M. Guilbaud, M. Kilpatrick, W. Li, B. Michlin, B.P. Padley, J. Roberts, J. Rorie, W. Shi, Z. Tu, J. Zabel, A. Zhang

University of Rochester, Rochester, USA

A. Bodek, P. de Barbaro, R. Demina, Y.t. Duh, J.L. Dulemba, C. Fallon, T. Ferbel, M. Galanti, A. Garcia-Bellido, J. Han, O. Hindrichs, A. Khukhunaishvili, K.H. Lo, P. Tan, R. Taus, M. Verzetti

Rutgers, The State University of New Jersey, Piscataway, USA

A. Agapitos, J.P. Chou, Y. Gershtein, T.A. Gómez Espinosa, E. Halkiadakis, M. Heindl, E. Hughes, S. Kaplan, R. Kunnawalkam Elayavalli, S. Kyriacou, A. Lath, R. Montalvo, K. Nash, M. Osherson, H. Saka, S. Salur, S. Schnetzer, D. Sheffield, S. Somalwar, R. Stone, S. Thomas, P. Thomassen, M. Walker

University of Tennessee, Knoxville, USA

A.G. Delannoy, J. Heideman, G. Riley, K. Rose, S. Spanier, K. Thapa

Texas A&M University, College Station, USA

O. Bouhali⁷², A. Castaneda Hernandez⁷², A. Celik, M. Dalchenko, M. De Mattia, A. Delgado, S. Dildick, R. Eusebi, J. Gilmore, T. Huang, T. Kamon⁷³, S. Luo, R. Mueller, Y. Pakhotin, R. Patel, A. Perloff, L. Perniè, D. Rathjens, A. Safonov, A. Tatarinov

Texas Tech University, Lubbock, USA

N. Akchurin, J. Damgov, F. De Guio, P.R. Duderov, S. Kunori, K. Lamichhane, S.W. Lee, T. Mengke, S. Muthumuni, T. Peltola, S. Undleeb, I. Volobouev, Z. Wang

Vanderbilt University, Nashville, USA

S. Greene, A. Gurrola, R. Janjam, W. Johns, C. Maguire, A. Melo, H. Ni, K. Padeken, J.D. Ruiz Alvarez, P. Sheldon, S. Tuo, J. Velkovska, M. Verweij, Q. Xu

University of Virginia, Charlottesville, USA

M.W. Arenton, P. Barria, B. Cox, R. Hirosky, M. Joyce, A. Ledovskoy, H. Li, C. Neu, T. Sinthuprasith, Y. Wang, E. Wolfe, F. Xia

Wayne State University, Detroit, USA

R. Harr, P.E. Karchin, N. Poudyal, J. Sturdy, P. Thapa, S. Zaleski

University of Wisconsin - Madison, Madison, WI, USA

M. Brodski, J. Buchanan, C. Caillol, D. Carlsmith, S. Dasu, L. Dodd, S. Duric, B. Gomber, M. Grothe, M. Herndon, A. Hervé, U. Hussain, P. Klabbers, A. Lanaro, A. Levine, K. Long, R. Loveless, T. Ruggles, A. Savin, N. Smith, W.H. Smith, N. Woods

†: Deceased

1: Also at Vienna University of Technology, Vienna, Austria

2: Also at IRFU, CEA, Université Paris-Saclay, Gif-sur-Yvette, France

3: Also at Universidade Estadual de Campinas, Campinas, Brazil

4: Also at Federal University of Rio Grande do Sul, Porto Alegre, Brazil

5: Also at Université Libre de Bruxelles, Bruxelles, Belgium

6: Also at Institute for Theoretical and Experimental Physics, Moscow, Russia

7: Also at Joint Institute for Nuclear Research, Dubna, Russia

8: Now at Cairo University, Cairo, Egypt

9: Also at Fayoum University, El-Fayoum, Egypt

10: Now at British University in Egypt, Cairo, Egypt

11: Now at Ain Shams University, Cairo, Egypt

12: Also at Department of Physics, King Abdulaziz University, Jeddah, Saudi Arabia

13: Also at Université de Haute Alsace, Mulhouse, France

14: Also at Skobeltsyn Institute of Nuclear Physics, Lomonosov Moscow State University, Moscow, Russia

15: Also at Tbilisi State University, Tbilisi, Georgia

16: Also at CERN, European Organization for Nuclear Research, Geneva, Switzerland

17: Also at RWTH Aachen University, III. Physikalisches Institut A, Aachen, Germany

18: Also at University of Hamburg, Hamburg, Germany

19: Also at Brandenburg University of Technology, Cottbus, Germany

20: Also at Institute of Nuclear Research ATOMKI, Debrecen, Hungary

21: Also at MTA-ELTE Lendület CMS Particle and Nuclear Physics Group, Eötvös Loránd University, Budapest, Hungary

22: Also at Institute of Physics, University of Debrecen, Debrecen, Hungary

23: Also at Indian Institute of Technology Bhubaneswar, Bhubaneswar, India

24: Also at Institute of Physics, Bhubaneswar, India

25: Also at Shoolini University, Solan, India

26: Also at University of Visva-Bharati, Santiniketan, India

27: Also at Isfahan University of Technology, Isfahan, Iran

28: Also at Plasma Physics Research Center, Science and Research Branch, Islamic Azad University, Tehran, Iran

- 29: Also at Università degli Studi di Siena, Siena, Italy
- 30: Also at International Islamic University of Malaysia, Kuala Lumpur, Malaysia
- 31: Also at Malaysian Nuclear Agency, MOSTI, Kajang, Malaysia
- 32: Also at Consejo Nacional de Ciencia y Tecnología, Mexico City, Mexico
- 33: Also at Warsaw University of Technology, Institute of Electronic Systems, Warsaw, Poland
- 34: Also at Institute for Nuclear Research, Moscow, Russia
- 35: Now at National Research Nuclear University 'Moscow Engineering Physics Institute' (MEPhI), Moscow, Russia
- 36: Also at St. Petersburg State Polytechnical University, St. Petersburg, Russia
- 37: Also at University of Florida, Gainesville, USA
- 38: Also at P.N. Lebedev Physical Institute, Moscow, Russia
- 39: Also at California Institute of Technology, Pasadena, USA
- 40: Also at Budker Institute of Nuclear Physics, Novosibirsk, Russia
- 41: Also at Faculty of Physics, University of Belgrade, Belgrade, Serbia
- 42: Also at INFN Sezione di Pavia ^a, Università di Pavia ^b, Pavia, Italy
- 43: Also at University of Belgrade, Faculty of Physics and Vinca Institute of Nuclear Sciences, Belgrade, Serbia
- 44: Also at Scuola Normale e Sezione dell'INFN, Pisa, Italy
- 45: Also at National and Kapodistrian University of Athens, Athens, Greece
- 46: Also at Riga Technical University, Riga, Latvia
- 47: Also at Universität Zürich, Zurich, Switzerland
- 48: Also at Stefan Meyer Institute for Subatomic Physics (SMI), Vienna, Austria
- 49: Also at Gaziosmanpasa University, Tokat, Turkey
- 50: Also at Adiyaman University, Adiyaman, Turkey
- 51: Also at Istanbul Aydin University, Istanbul, Turkey
- 52: Also at Mersin University, Mersin, Turkey
- 53: Also at Piri Reis University, Istanbul, Turkey
- 54: Also at Ozyegin University, Istanbul, Turkey
- 55: Also at Izmir Institute of Technology, Izmir, Turkey
- 56: Also at Marmara University, Istanbul, Turkey
- 57: Also at Kafkas University, Kars, Turkey
- 58: Also at Istanbul University, Faculty of Science, Istanbul, Turkey
- 59: Also at Istanbul Bilgi University, Istanbul, Turkey
- 60: Also at Hacettepe University, Ankara, Turkey
- 61: Also at Rutherford Appleton Laboratory, Didcot, United Kingdom
- 62: Also at School of Physics and Astronomy, University of Southampton, Southampton, United Kingdom
- 63: Also at Monash University, Faculty of Science, Clayton, Australia
- 64: Also at Bethel University, St. Paul, USA
- 65: Also at Karamanoğlu Mehmetbey University, Karaman, Turkey
- 66: Also at Utah Valley University, Orem, USA
- 67: Also at Purdue University, West Lafayette, USA
- 68: Also at Beykent University, Istanbul, Turkey
- 69: Also at Bingol University, Bingol, Turkey
- 70: Also at Sinop University, Sinop, Turkey
- 71: Also at Mimar Sinan University, Istanbul, Istanbul, Turkey
- 72: Also at Texas A&M University at Qatar, Doha, Qatar
- 73: Also at Kyungpook National University, Daegu, Korea